Stability Analysis With LMI Based Distributed H∞ Controller for Vehicle Platooning Under Random Multiple Packet Drops

Citation for published version:
Halder, K, Gillam, L, Dixit, S, Mouzakitis, A & Fallah, S 2022, 'Stability Analysis With LMI Based Distributed H∞ Controller for Vehicle Platooning Under Random Multiple Packet Drops', *IEEE Transactions on Intelligent Transportation Systems*, vol. 23, no. 12, pp. 23517 - 23532. https://doi.org/10.1109/TITS.2022.3196183

Digital Object Identifier (DOI):
10.1109/TITS.2022.3196183

Published In:
IEEE Transactions on Intelligent Transportation Systems

Stability Analysis With LMI Based Distributed H_∞ Controller for Vehicle Platooning Under Random Multiple Packet Drops

Kaushik Halder, Lee Gillam, Shilp Dixit, Alexandros Mouzakitis, and Saber Fallah

***Abstract*— This paper proposes a discrete time distributed state feedback controller design strategy for a homogenous vehicle platoon system with undirected network topology which is resilient to both external disturbances and random consecutive network packet drop. The system incorporates a distributed state feedback controller design by satisfying bounded H_∞ norm using Lyapunov-Krasovskii based linear matrix inequality (LMI) approach that ensures internal stability and performance. The effect of packet drops on internal stability in terms of stability margin are studied for a homogenous vehicle platoon system with undirected network topology and external disturbance. The variation of stability margin, representing absolute value of least stable close-loop pole, is also studied for two common undirected network topologies for vehicle platooning, i.e., bidirectional predecessor following (BPF) and bidirectional predecessor leader following (BPLF) topologies by varying platoon members, packet drop rates with number of contiguous packets dropped. Results demonstrate that the control strategy best satisfies the requirement of maintaining a desired inter-vehicular distance with constant spacing policy and leader trajectory using two network topologies: BPF and BPLF. We show how these topologies are robust in terms of ensuring internal stability and performance to maintain cooperative motion of vehicle platoon system with different number of followers, random multiple consecutive packet drops and external disturbance.**

***Index Terms*— Vehicle platoon, LMI, distributed H_∞ control, stability margin, random multiple packet drops.**

I. Introduction

VEHICLE platoon systems manage groups of two or more connected autonomous vehicles (CAVs) travelling together, for the most part, in a single lane of a highway. A platoon comprises of a first vehicle called the leader and other vehicles referred to as followers. Vehicles in a platoon travel with a commonly agreed speed and maintain pre-specified and short inter-vehicular distances for which multi vehicle co-operation is critical [1], [2]. The benefits of small inter-vehicular distances in a platoon include road safety, highway utility, and fuel economy [3], [4]. A vehicle platoon system can be referred to as homogeneous or heterogeneous, depending on the dynamics of the member vehicles [5]–[7]. A vehicle platoon is called homogeneous if the dynamics of its member vehicles are identical, otherwise, it is heterogeneous [6], [7].

A. Related Works on Vehicle Platooning With Different Network Topologies

To ensure internal stability by maintaining cooperative motion such as specified inter-vehicular distance, desired speed etc. among the vehicles in a platoon system, several researcher groups have designed platoon control systems under various communication topologies as reported in [2], [6], [8]. In general, the vehicles in a platoon exchange their information with other platoon members using wireless communication systems to support vehicle-to-vehicle (V2V) and vehicle-to-infrastructure (V2I) communication to maintain the cooperative motion [1]. The information exchange, through wireless communication, amongst the vehicles in a platoon can be distinguished by the network topology or information flow topology (IFT) [6]–[9]. The IFT can be either directed or undirected. A network topology is called undirected if communication between all pairs of connected vehicles in a platoon are bidirectional, otherwise it is directed. Typical examples of directed and undirected network topologies are predecessor following (PF), two PF (TPF), predecessor leader following (PLF) [6], [8] and bidirectional PF (BPF), two BPF (TBPF), bidirectional PLF (BPLF) [6]–[8], and all-to-all [10], respectively. The importance of various network topologies in vehicle platoon systems has been reported in [6], [8]. Amongst the various network topologies used in vehicle platoon systems, the analysis of platoon control systems with undirected topology has piqued the interest of several researchers because vehicles in a platoon can share more information amongst themeselves thus improving the system's performance as reported in [6], [7], [9], [11]–[14]. However, inherent properties of wireless communication networks in platoon systems may lead to packet drops and/or delays in data transmissions among the vehicles [8], [15], [16] since reliability highly depends on bandwidth allocation, signal

Manuscript received 5 July 2021; revised 14 March 2022; accepted 20 July 2022. This work was supported by Jaguar Land Rover and the U.K.-Engineering and Physical Sciences Research Council (EPSRC) under Grant EP/N01300X/1 as part of the jointly funded Towards Autonomy: Smart and Connected Control (TASCC) Program. The Associate Editor for this article was P. Kachroo. *(Corresponding author: Saber Fallah.)*

Kaushik Halder was with the CAV-Laboratory, Department of Mechanical Engineering Sciences, University of Surrey, Guildford GU2 7XH, U.K. He is now with the School of Informatics, University of Edinburgh, Edinburgh EH8 9AB, U.K.

Lee Gillam is with the Department of Computer Science, University of Surrey, Guildford GU2 7XH, U.K.

Shilp Dixit was with the CAV-Laboratory, Department of Mechanical Engineering Sciences, University of Surrey, Guildford GU2 7XH, U.K. He is now with the Vay Technology, 12099 Berlin, Germany.

Alexandros Mouzakitis is with Jaguar Land Rover Ltd., Coventry CV3 4LF, U.K.

Saber Fallah is with the CAV-Laboratory, Department of Mechanical Engineering Sciences, University of Surrey, Guildford GU2 7XH, U.K. (e-mail: s.fallah@surrey.ac.uk).

Digital Object Identifier 10.1109/TITS.2022.3196183

strength, etc. [17]. Such network issues, i.e., packet drop or communication delay, may cause performance degradation in terms of stability and control loop performance leading to instability of the vehicle platoon systems [15], [18], [19]. Therefore, the challenge is to design a platoon control system that ensures stability and maintains desired performance, keeping appropriate desired speed and pre-specified inter-vehicular distance in a vehicle platoon system and being resilient against network issues such as packet drop and especially, under multiple consecutive packet drops.

B. Related Works on Controller Design Under Packet Drop and/or Delay for Vehicle Platooning

Various controller design approaches such as model predictive control (MPC) [20], [21], sliding mode control (SMC) [13], [22], adaptive control [10], H_∞ control [7], [7], [9] etc. have been established to ensure closed-loop stability and cooperative motion either for homogeneous [9], [10], [23]–[25] or heterogeneous [20], [26], [27] vehicle platoon systems with and without complexities like external disturbances (due to wind gust, road slope etc.) [7], [13], [28], parametric uncertainties (due to, engine time constant, change in mass under different load etc.) [13], network imperfections such as packet drop [9], [14], [29] and communication delay [27], [28]. For example, distributed MPC has been designed for heterogeneous vehicle platooning with unidirectional topology, i.e. directed in [20]. SMC based control strategy has been designed for vehicle platoon systems using car-following theory in [22]. A distributed adaptive control strategy has been proposed to ensure string stability for vehicle platoon system with dynamic uncertainty in [30]. A distributed H_∞ controller design methodology has been proposed for uncertain heterogeneous platoon systems with undirected topology in [12]. To ensure stability and robustness of the homogeneous platoons with undirected topology and external disturbances, an LMI based distributed H_∞ controller has been designed in [7]. An adaptive control strategy has been developed to ensure cooperative motion by reducing demands on the communication network, i.e., reducing the network load among the member vehicles in a homogeneous vehicle platoon system, modelled as a synchronisation problem of multi-agent systems in [10]. The internal stability in terms of stability margin for continuous time homogeneous and heterogeneous vehicle platoon systems with undirected topology were analysed in [6], [11], [31] and [2] respectively. The works in [2], [6], [11], [32], and [31] measured stability margin as the absolute value of the real part of the least stable closed-loop eigenvalue/pole in the continuous time domain, i.e., in the s-plane and proposed methodologies like asymmetric control, mistuning of symmetric control, and reduction of tree depth by extending information flow to improve stability margin of closed-loop platoon systems, respectively. An interested reader can refer to [16], which contains a detailed survey on vehicle platoon stability and control issues, including homogeneous and heterogeneous platoons, formation geometry i.e. spacing policies, various IFTs e.g. directed and undirected, stability and performance analysis i.e. internal and string stability, robustness analysis with various platoon control strategies etc. However, none of these methods ensure the internal stability of vehicle platoon system under network imperfections such as packet drop and/or communication delay. To achieve internal stability under such conditions with low/high communication latency, a decentralised MPC has been designed for longitudinal platoon control problem in [21]. In [29], an LMI based distributed state feedback controller has been designed to achieve co-ordinated motion under random packet drop for vehicle platooning modelled as a multi-agent control problem. An LMI based finite time control strategy has been proposed for analysing stability and robustness of multi platoons with time varying delays in [33]. For heterogeneous vehicle platooning with PF topology and under packet drop and delay, a two-layered control technique within a distributed MPC and state feedback control framework with multi rate sampling has been proposed in [34]. In [35], an adaptive event-triggered control strategy was proposed and both internal and string stability of vehicle platoons with packet drop and communication delay were investigated. Internal stability and string stability for homogeneous vehicle platoons were investigated under limited communication range with random packet drop in [23] and with both random packet drop and time varying communication delay in [36], respectively. Analysis of string stability and control performances of a platoon under packet drop and communication delay has been reported in [15], [37] and [38], [39], respectively. However, in contrast to the above mentioned research works, very few researchers have proposed control strategies for analysing internal stability, string stability and robust performance of the vehicle platoon systems under both networked packet drop or delay and parametric uncertainty or external disturbances [9], [14], [19], [25], [27], [40]. An LMI based distributed H_∞ controller has been designed for heterogeneous vehicle platoon systems under parametric uncertainties, external disturbances, and communication delays in [27]. However, the method proposed in [27] only considers PLF network topology (i.e., unidirectional) for communication among platoon vehicles. As an extension of [27], an LMI based distributed H_∞ controller design methodology has been proposed to analyse robustness, and cooperative motion for homogeneous vehicle platooning with generic network structure (i.e., both unidirectional and bidirectional) under random single packet drop and external disturbances in [14]. H_∞ control strategy has been developed for homogeneous platoon with external distubances, random packet drop and communication delay in [25]. The analytical solution of robustness analysis was obtained and LMI based distributed H_∞ controller was designed with a dimension of single vehicle for homogeneous vehicle platoon systems under undirectional network topology, random single packet drop, and external disturbances in [9]. However, the methodologies of [9] and [14] do not ensure stability and control loop performances for vehicle platoon systems under multiple consecutive packet drops. In contrast to the literature described above, this paper proposes an LMI based distributed controller design methodology for homogeneous vehicle platoon systems with generic undirected network topologies, i.e., bidirectional, for communication between vehicles under random multiple consecutive packet drops and external disturbances in discrete time. In addition, the designed controller is also used to analyse internal stability, represented by stability margin, of a platoon control system under random consecutive packet drops and external disturbances. Thus, this paper extends the research, reported in [6], [7] and [9], [14], where a distributed controller was implemented to ensure internal stability and robustness for the homogeneous vehicle platoon system either with perfect communication (i.e., without packet drop) or with random single packet drop only, respectively.

C. Contribution of the Present Work

In this paper, a discrete time distributed H_∞ controller has been designed for cooperative driving of longitudinal dynamics of a linear time invariant (LTI) homogeneous platoon with external disturbances and random consecutive packet drops modelled as probabilistic Bernoulli distribution. The designed controller is then used to analyse the stability margin for such a system. As in [7], [9], [10], [14], here, the synchronisation problem of multi-agent system using algebraic graph theory is used to transform homogeneous vehicle platoon control problem under multiple consecutive packet drops and external disturbance. The contributions of the paper are reported as follows:

- Lyapunov-Krasovskii based LMI approach is used to obtain the controller gains with the satisfaction of certain bounded H_∞ norm which ensures the mean square stability (MSS) and maintains desired inter-vehicular distances for homogeneous platoon systems with multiple consecutive packet drops and external disturbance.
- In contrast to [25], for reducing the computational complexity for the tuning of control gains, a methodology to reduce the size of the resultant LMI (mentioned above) to the dimensions of an LMI on the single vehicle dynamics is proposed. This methodology ensures MSS and bounded H_∞ norm for entire platoon system with undirected topologies, multiple consecutive packet drops and external disturbance.
- In the discrete time domain, i.e., in the z-domain, the stability margin is measured by the absolute value of the least stable closed-loop eigenvalue to the circumference of the unit circle. This concept is used for the internal stability analysis of a platoon system under undirected topologies (e.g., BPF and BPLF), multiple consecutive packet drops and external disturbance with the designed controller. This contrasts with the continuous time domain analysis performed in [6], [11], [31], [32] where the value of the real part of the least stable closed-loop eigenvalue in the negative half of the s-plane was checked. Additionally, for different platoon members, the effects of different packet drop rate on the stability margin of the platoon system with two different network topologies (e.g., BPF and BPLF) and external disturbance, including multiple packet drops where packets are dropped consecutively, are also studied. Furthermore, the effects of different sampling time (T_s) on the internal stability of vehicle platoon control systems with BPF and BPLF topologies are studied to understand robustness capability in terms of stability and performance of the proposed controller design methodology. To the best of our knowledge, the above-mentioned studies have not been investigated yet in the contemporary literature. Therefore, the current work numerously extends the results by considering external disturbance, different packet drop rate, and sampling time of [6], [11] where stability and scalability were investigated for homogeneous platoon systems without external disturbance and under perfect communication network (i.e., without random packet drop) in continuous time domain.

The rest of the paper is organised as follows: Section II describes platoon modelling and control objectives of platoons for the synchronisation problem under consecutive packet drop. Then, to achieve the control objectives for a platoon, the LMI based distributed controller design approach for satisfying internal stability is described in Section III. Numerical and simulation results are shown in Section IV to analyse the effectiveness of the proposed method. Conclusions are presented in Section V. The paper also has an Appendix, containing a systematic proof of the core Theorems.

Notations. Here, some standard mathematical notations used throughout the paper are introduced for convenience. $\mathbb{R}^n$ and $\mathbb{R}^{n\times n}$, are the n-dimensional real Euclidean space and the $n \times n$ real matrix space, respectively. $\boldsymbol{M}^{-1}$ ($\boldsymbol{M}^T$) denotes the inverse (transpose) of a square matrix $\boldsymbol{M}$. $\boldsymbol{M} < \boldsymbol{0}$ ($\boldsymbol{M} > \boldsymbol{0}$) is a strictly negative (positive) definite matrix, whereas, $\boldsymbol{M} = \boldsymbol{M}^T \leq \boldsymbol{0}$ ($\boldsymbol{M} = \boldsymbol{M}^T \geq \boldsymbol{0}$) denotes a symmetric negative (positive) semi-definite matrix. $\lambda_i(\boldsymbol{M})$ is the i^{th} eigenvalue of a symmetric matrix $\boldsymbol{M}$ after they have been sorted in ascending order, and $\lambda_{\min}(\boldsymbol{M})$ denotes the minimum eigenvalue of $\boldsymbol{M}$. $\boldsymbol{I}_n$ is the unit matrix in the $n \times n$ real matrix space. The symbol $(*)$ represents the symmetric elements of a symmetric matrix and $(\otimes)$ represents the Kronecker product between two matrices. Given a random variable ζ, $\mathbb{E}(\zeta)$ denotes its expected value (mean value).

II. Modelling and Control Objectives of Vehicle Platoon Systems

In this paper, the platoon control problem is considered as a synchronisation problem of a networked dynamical system with a pinner node [7], [9], [10], [41] where a set of agents (i.e., follower vehicles) defined by nodes interact among themselves through a network and these nodes are controlled in such a way that the dynamics of all nodes (i.e., follower vehicles) converge towards the pinner node (i.e., the leader of a platoon). This section describes the modelling of the platoon network topology and longitudinal dynamics of the vehicles in a platoon represented by graph nodes. For the synchronisation problem of vehicle platoon systems with communication topology and random packet drop, it is assumed that the follower vehicles receive information from the leader, i.e., the pinner node, but the leader will not receive any information from the followers as reported in [9], [10], [14].

A. Modelling of the Network Topology and Random Packet Drop for Vehicle Platooning

The graph $\mathcal{G}_N = (\mathcal{V}_N,\mathcal{E}_N)$ represents the communication topology of the N followers (nodes) where $\mathcal{V}_N =$

$\{1, 2, \ldots, N\}$ denotes a set of nodes or vertices and $\mathcal{E}_N \subseteq \mathcal{V}_N \times \mathcal{V}_N$ is the set of edges or arcs. The pair $(i, j) \in \mathcal{E}_N$ indicates that the i^{th} vehicle receives the information from the j^{th} vehicle. Based on the edges $\mathcal{E}_N$, an adjacency matrix $\mathcal{A}_N = [\tilde{a}_{ij}] \in \mathbb{R}^{N\times N}$ can be defined. The generic entry $\tilde{a}_{ij}$ of the adjacency matrix defines $\tilde{a}_{ij} = 1$ when $(i, j) \in \mathcal{E}_N$ and $\tilde{a}_{ij} = 0$ otherwise, i.e., $\tilde{a}_{ij} = 1$ implies that the i^{th} vehicle receives the j^{th} vehicle's information while $\tilde{a}_{ii} = 0$ represents no self-loop in the network. The degree $\mathcal{D}_N$ of the graph is represented by the number of edges pointing to the follower. For such a case the Laplacian matrix $\mathcal{L} = [l_{ij}] \in \mathbb{R}^{N\times N}$ can be represented by $\mathcal{L} = \mathcal{D}_N - \mathcal{A}_N$ where $l_{ii} = \sum_{j\neq i} \tilde{a}_{ij}$ and $l_{ij} = -\tilde{a}_{ij}\ \forall\ i \neq j$. The neighbour set of the node i in the followers is represented by $\mathbb{N}_i$ i.e., $\mathbb{N}_i = \{j \in \mathcal{V}_N \mid \tilde{a}_{ij} = 1\}$. If the network topology considers the leader (i.e., leader of the platoon or pinner of the network) then the graph $\mathcal{G}_N$ is augmented with node 0 and the modified graph is $\mathcal{G}_{N+1} = (\mathcal{V}_{N+1}, \mathcal{E}_{N+1})$ where $\mathcal{V}_{N+1} = \{0, 1, \ldots, N\}$ and $\mathcal{E}_{N+1} \subseteq \mathcal{V}_{N+1} \times \mathcal{V}_{N+1}$, also representing the pinner of the network. The corresponding adjacency matrix is $\mathcal{A}_{N+1} = [\tilde{a}_{ij}] \in \mathbb{R}^{(N+1)\times(N+1)}$ with $\tilde{a}_{0j} = 0$, $j = 1, 2, \ldots, N$, indicates that the followers are not sending information to the leader, $\tilde{a}_{i0} = 1$, $i = 1, 2, \ldots, N$ indicates that the followers are receiving information from the leader and finally $\tilde{a}_{i0} = 1$ indicates otherwise. $\mathcal{P} = diag\{p_1, p_2, \ldots, p_N\}$ represents the pinning matrix which defines connections between each follower and the leader where $p_i = 1, i = 1, 2, \ldots, N$ if node i is obtaining the information from the leader, i.e., node i is pinned to the leader and $p_i = 0$ otherwise. The leader-accessible set of node i can be defined as:

$$\mathcal{P}_i = \begin{cases} \{0\} & \text{if } p_i = 1, \\ \emptyset & \text{if } p_i = 0. \end{cases} \tag{1}$$

This paper considers undirected topologies, i.e., $i \in \mathbb{N}_i \Leftrightarrow j \in \mathbb{N}_j$, $\forall i,\ j \in \mathcal{V}_N$. Next, we assume the stochastic variable $\theta_{ij}(k) \in \{0, 1\}$ is satisfying a Bernoulli distribution representing packet drop in the communication network among the vehicles in a platoon. $\theta_{ij}(k) = 0$ represents the i^{th} follower receives a packet from follower j while $\theta_{ij}(k) = 1$ represents packet drop or data loss. Thus, the following conditions hold:

$$Prob(\theta_{ij}(k) = 1) = \mathbb{E}(\theta_{ij}(k)) = r, \forall i \neq j, \tag{2a}$$
$$\mathbb{E}(1 - \theta_{ij}(k)) = 1 - r, \forall i \neq j, \tag{2b}$$

where, r defines the mean packet drop rate in the communication network among the vehicles.

B. Modelling of the Longitudinal Vehicle Dynamics

In a vehicle platoon system, the nonlinear longitudinal dynamics of the member vehicles can be represented by a third order linearized differential equation due to its satisfactory trade-off between accuracy and simplicity [7], [9]. The third order model of i^{th} vehicle with disturbance input in homogeneous platoon considering the states $\boldsymbol{x}_i^T(t) = [s_i,\ v_i,\ a_i]$, $i = 1, 2, \ldots, N$ is represented in state space form as:

$$\dot{\boldsymbol{x}}_i(t) = \boldsymbol{A}\boldsymbol{x}_i(t) + \boldsymbol{B}u_i(t) + \boldsymbol{B}\omega_i(t), \tag{3a}$$
$$y_i(t) = \boldsymbol{C}\boldsymbol{x}_i(t), \tag{3b}$$

where, $u_i(t) \in \mathbb{R}$, $\omega_i(t) \in \mathbb{R} \in L_2[0, \infty)$ and $y_i(t) \in \mathbb{R}$ are the system input, the exogenous disturbance, and output, respectively, while the system matrices are

$$\boldsymbol{A} = \begin{bmatrix} 0 & 1 & 0 \\ 0 & 0 & 1 \\ 0 & 0 & -\frac{1}{\tau} \end{bmatrix}, \quad \boldsymbol{B} = \begin{bmatrix} 0 \\ 0 \\ \frac{1}{\tau} \end{bmatrix}, \quad \boldsymbol{C} = \begin{bmatrix} 1 & 0 & 0 \end{bmatrix}. \tag{4}$$

In (4), s_i, v_i, a_i and τ represent position, velocity, acceleration, and time constant of the power train of the i^{th} follower vehicle in a platoon, respectively. The equivalent discretised system using forward Euler discretisation method of its continuous time version (4) with specified sampling time T_s is represented as [42]–[44]:

$$\boldsymbol{x}_i(k+1) = \boldsymbol{A}_d\boldsymbol{x}_i(k) + \boldsymbol{B}_d u_i(k) + \boldsymbol{B}_d\omega_i(k), \tag{5a}$$
$$y_i(k) = \boldsymbol{C}\boldsymbol{x}_i(k), \tag{5b}$$

where, $\boldsymbol{A}_d = \boldsymbol{I}_3 + \boldsymbol{A}T_s$ and $\boldsymbol{B}_d = \boldsymbol{B}T_s$.

C. Control Objectives of Vehicle Platoon Systems

In general, two different strategies such as constant spacing policy (CSP) and constant time headway policy (CTHP) are used for platoon stability and spacing control problem. CSP ensures that the distance between successive vehicles is kept constant, whereas, the inter-vehicle spacing is a function of velocity of vehicles under CTHP [6], [40], [45]. Although, CTHP is simpler to implement and provide more advantages for analysing string stability under simple IFT than CSP [40], [46], but CSP has higher traffic capacity over CTHP [6], [45] for vehicle platooning. Here, we consider CSP as in [2], [6], [9], [10], [12], [14], [20], [24], [47], which means that vehicles are controlled to follow a leading vehicle in a rigid formation ensuring stability and robust performance under random consecutive packet drop and/or communication delay and external disturbances. The control objective of the platoon is categorised in two ways [9], [10] (*i*) to impose leader velocity to all followers and (*ii*) to maintain specified inter-vehicular distance between consecutive vehicles in a platoon with a given spacing policy [7], [9], [10]. If $d_{i,i-1}$, $i = 1, 2, \ldots, N$ represents the desired inter-vehicular distance between i^{th} vehicle and its predecessor with a constant spacing policy [1], [5], [13], then the aim of the platoon control is to find $u_i(k)$ in (5) such that,

$$\lim_{k\to\infty} \| v_i(k) - v_0(k) \| = 0, \tag{6a}$$
$$\lim_{k\to\infty} \| s_i(k) - s_{i-1}(k) - d_{i,i-1} \| = 0, \quad \forall i = 1, 2, \ldots, N, \tag{6b}$$

where, v_0 represents the velocity of the leader. This paper considers the leader of a platoon is travelling with a constant speed, i.e., $a_0 = 0$ [7], [9], [10].

If $d_{i,0}$ is the desired distance between the leader and the i^{th} follower, i.e., $d_{i,0} = \sum_{m=1}^{i} d_{m,m-1}$, then the second objective of (6) can be re-written as $\lim_{k\to\infty} \| s_i(k) - s_0(k) - d_{i,0} \| = 0$, which together with the first objective (6a) represents consensus or synchronisation problem where the pinner is represented by the leader vehicle which provides the reference trajectory. Therefore, if the tracking error for the i^{th} follower is represented by $\hat{\boldsymbol{x}}_i(k) = [\hat{s}_i(k), \hat{v}_i(k), \hat{a}_i(k)]^T$, where $\hat{s}_i(k) = s_i(k) - s_0(k) - d_{i,0}$, $\hat{v}_i(k) = v_i(k) - v_0(k)$ and $\hat{a}_i(k) = a_i(k) - a_0(k)$ then (6) becomes

$$\| \hat{\boldsymbol{x}}_i(k) \| \to 0 \quad \text{when} \quad k \to \infty, \forall i = 1, 2, \ldots, N. \tag{7}$$

It is noted that eqn. (7) does not consider *(i)* random packet drop in the communication channel which allows the expected value of $\hat{\boldsymbol{x}}_i(k) \to 0$ as $k \to \infty, \forall i = 1, 2, \ldots, N$ and *(ii)* effect of external disturbances $w_i(t)$ on the output dynamics $y_i(t)$, $i = 1, 2, \ldots N$.

To address these issues, this paper considers mean square stability (MSS) and H_∞ norm bound as platoon control objectives under random consecutive packet drop and external disturbances. The platoon control objectives under MSS and bounded H_∞ norm has been described as follows:

Definition 1: If $\lim_{k\to\infty} \mathbb{E}(\| \boldsymbol{X}(k) \|^2) = 0$ for any initial state $\boldsymbol{X}(0) \in \mathbb{R}^{3N}$, then tracking error $\boldsymbol{X}(k)$ is said to be MSS [9], [41].

Definition 2: If the closed-loop system is MSS and following hold [9], [48]:

$$\sum_{k=0}^{\infty} \mathbb{E}(\| \boldsymbol{Y}(k) \|^2) \leqslant \gamma^2 \sum_{k=0}^{\infty} \mathbb{E}(\| \boldsymbol{W}(k) \|^2), \tag{8}$$

for all $\boldsymbol{X}(0) = 0$ and $\boldsymbol{W}(k) = [w_1^T(k), w_2^T(k), \ldots, w_N^T(k)]^T \neq 0$, then there exist a bounded H_∞ norm $\gamma > 0$, in the output error dynamics $\boldsymbol{Y}(k)$.

The detail explanation of Definition 1 and 2 can be found in [9] (see Definition 2 and 3 of [9]).

To achieve the platoon control objective (7) by imposing MSS and H_∞ norm bound, we define stack of state tracking error as $\boldsymbol{X}(k) = [\hat{\boldsymbol{x}}_1^T(k), \hat{\boldsymbol{x}}_2^T(k), \ldots, \hat{\boldsymbol{x}}_N^T(k)]^T$ and output tracking error as $\boldsymbol{Y}(k) = [\hat{s}_1(k), \hat{s}_2(k), \ldots, \hat{s}_N(k)]^T = (\boldsymbol{I}_N \otimes \boldsymbol{C})\boldsymbol{X}(k)$.

D. Modelling of Consecutive Packet Drop for Vehicle Platoon Systems

The network packet drop is modelled as a Bernoulli distribution. Let, $\bar{\boldsymbol{x}}_i(k)$ be the augmented state tracking error of the i^{th} follower which can be used by the j^{th} follower at kT_s instant, since j^{th} follower knows whether the information from i^{th} follower has been received or not in the form of a packet. Then $\bar{\boldsymbol{x}}_i(k)$ can be represented under consecutive packet drop or consecutive sample delay, denoted as stochastic known variable $\beta_k = \beta(k)$ which is bounded within $1 \leqslant \beta_k \leqslant \delta_{max}$ [41]:

$$\bar{\boldsymbol{x}}_i(k) = (1 - \theta_{ij}(k))\hat{\boldsymbol{x}}_i(k) + \theta_{ij}(k)\hat{\boldsymbol{x}}_i(k - \beta_k), \tag{9}$$

correspondingly,

$$\bar{\boldsymbol{x}}_j(k) = (1 - \theta_{ji}(k))\hat{\boldsymbol{x}}_j(k) + \theta_{ji}(k)\hat{\boldsymbol{x}}_j(k - \beta_k), \tag{10}$$

where, maximum packet drop or sample delay (δ_{max}) is the known integer. Similar to [9], [14], [41], this paper assumes $\theta_{ij}(k) = \theta_{ji}(k)$, which defines that a specific link failure affects the consecutive packet drops in both directions with mean packet drop rate r as described in (2).

III. Stability Analysis and Controller Design for Vehicle Platoons Under Consecutive Packet Drop

A. Controller Design Under Random Consecutive Packet Drop

Considering the packet drop in the transmitted state vectors (9) and (10) among the vehicles in a platoon, the control law for each follower can be represented as:

$$u_i(k) = \boldsymbol{K} \sum_{j \in \mathbb{Q}_i} (\bar{\boldsymbol{x}}_i(k) - \bar{\boldsymbol{x}}_j(k)), \forall i = 1, 2, \ldots, N, \tag{11}$$

where, $\mathbb{Q}_i = \mathbb{N}_i \cup \mathcal{P}_i$ is the neighbour set of the follower i in the $\mathcal{G}_{N+1}$ graph and $\boldsymbol{K} = [-K_s, -K_v, -K_a]$ represents the identical controller gain for each follower vehicle since this paper considers homogenous platoon system [9].

Now, defining the stack of the augmented control action as $\boldsymbol{U}(k) = [u_1^T(k), u_2^T(k), \ldots, u_N^T(k)]^T$, the control law takes the form:

$$\boldsymbol{U}(k) = (\mathcal{L} + \mathcal{P}) \otimes \boldsymbol{K}[(1 - \theta_{ij}(k))\boldsymbol{X}(k) + (\theta_{ij}(k))\boldsymbol{X}(k - \beta_k)]. \tag{12}$$

The closed-loop dynamics of the state tracking error using the control law (12) for homogeneous platoon systems can be represented as:

$$\begin{aligned} \boldsymbol{X}(k+1) &= (\boldsymbol{I}_N \otimes \boldsymbol{A}_d)\boldsymbol{X}(k) + ((\mathcal{L} + \mathcal{P})(1 - \theta_{ij}(k)) \\ &\quad \otimes \boldsymbol{B}_d\boldsymbol{K})\boldsymbol{X}(k) + ((\mathcal{L} + \mathcal{P})\theta_{ij}(k) \otimes \boldsymbol{B}_d\boldsymbol{K}) \\ &\quad \times \boldsymbol{X}(k - \beta_k) + (\boldsymbol{I}_N \otimes \boldsymbol{B}_d)\boldsymbol{W}(k), \\ \boldsymbol{Y}(k) &= (\boldsymbol{I}_N \otimes \boldsymbol{C})\boldsymbol{X}(k). \end{aligned} \tag{13}$$

To achieve the control objectives (6) for the closed-loop system (13), the control gain need to be designed. An LMI approach to obtain the control gain satisfying the closed-loop system (13) to be MSS with a bounded H_∞ norm is described by the following theorem.

Theorem 1: Given system (13) with consecutive packet drop modelled as in (9)-(10) with mean packet drop rate r as in (2) and the control action (12), then closed-loop system is MSS satisfying bounded H_∞ norm if there exists $\boldsymbol{P} = \boldsymbol{P}^T = \boldsymbol{I}_N \otimes \boldsymbol{P}_0 > \boldsymbol{0} \in \mathbb{R}^{3N\times 3N}$, $\boldsymbol{Q} = \boldsymbol{Q}^T = \boldsymbol{I}_N \otimes \boldsymbol{Q}_0 > \boldsymbol{0}$, $\boldsymbol{R} = \boldsymbol{R}^T = \boldsymbol{I}_N \otimes \boldsymbol{R}_0 > \boldsymbol{0} \in \mathbb{R}^{3N\times 3N}$ and $\boldsymbol{Z} \in \mathbb{R}^{1\times 3}$ such that $\boldsymbol{\Pi} < \boldsymbol{0}$ in (14), shown at the bottom of the next page, hold, where, $\tilde{\boldsymbol{L}} = (\mathcal{L} + \mathcal{P})$, $\boldsymbol{P}^{-1} = \bar{\boldsymbol{P}}$, $\boldsymbol{Q}^{-1} = \bar{\boldsymbol{Q}}$, $\boldsymbol{R}^{-1} = \bar{\boldsymbol{R}}$, $\boldsymbol{P}^{-1}\boldsymbol{Q}\boldsymbol{P}^{-1} = \boldsymbol{\Xi}$, $\boldsymbol{P}^{-1}\boldsymbol{R}\boldsymbol{P}^{-1} = \boldsymbol{\Theta}$ and $\boldsymbol{K} = \boldsymbol{Z}\bar{\boldsymbol{P}}_0^{-1} = \boldsymbol{Z}\boldsymbol{P}_0 \in \mathbb{R}^{1\times 3}$ is the controller gain of (12).

The analytical proof of the Theorem 1 is presented in the Appendix.

It can be inferred that the dimension of LMI (14) in Theorem 1 is high, i.e., ($\boldsymbol{\Pi} = \mathbb{R}^{14N\times 14N}$) for large number of followers (N) in a platoon which is computationally expensive and may result in an infeasible and/or intractable problem. Therefore, to improve the computational efficiency, the idea of orthogonality [9] is used for decomposing the LMI (14) which is described in the following as Theorem 2 with reduced in dimension.

Theorem 2: Given closed-loop system (13) under consecutive packet drop modelled as in (10) with mean packet drop rate r (2) and the control action (12) is MSS satisfying bounded H_∞ norm $\gamma > 0$ if there exists $\boldsymbol{P}_0 = \boldsymbol{P}_0^T > \boldsymbol{0}$, $\boldsymbol{Q}_0 = \boldsymbol{Q}_0^T > \boldsymbol{0}$, $\boldsymbol{R}_0 = \boldsymbol{R}_0^T > \boldsymbol{0} \in \mathbb{R}^{3\times 3}$ $\forall\ \lambda_i \triangleq \lambda_i(\mathcal{L}+\mathcal{P})$, $i = 1, 2, \ldots, N$ such that $\tilde{\boldsymbol{\Pi}}_i < \boldsymbol{0}$ in (15), shown at the bottom of the page, hold, $\boldsymbol{P}_0{}^{-1} = \bar{\boldsymbol{P}}_0$, $\boldsymbol{Q}_0{}^{-1} = \bar{\boldsymbol{Q}}_0$, $\boldsymbol{R}_0{}^{-1} = \bar{\boldsymbol{R}}_0$, $\boldsymbol{P}_0{}^{-1}\boldsymbol{Q}_0\boldsymbol{P}_0{}^{-1} = \boldsymbol{\Xi}_0$, $\boldsymbol{P}_0{}^{-1}\boldsymbol{R}_0\boldsymbol{P}_0{}^{-1} = \boldsymbol{\Theta}_0$ and $\boldsymbol{K} = \boldsymbol{Z}\bar{\boldsymbol{P}}_0{}^{-1} = \boldsymbol{Z}\boldsymbol{P}_0 \in \mathbb{R}^{1\times 3}$ is the controller gain of (12).

The analytical proof of the Theorem 2 is presented in the Appendix.

Remark 1: The dimension of LMI (14) is scaled with the number of followers in a platoon. Therefore, high computational effort may require to obtain the solution from LMI (14) and also may results computationally infeasible and/or intractable problem when platoon system is with large number of followers. To overcome this problem, the LMI (15) is decomposed form of set of LMI (14) into a size of single vehicle rather than size of whole platoon system to obtain controller gain (12). The LMI $\tilde{\boldsymbol{\Pi}}_i$ in (15) is affine in λ_i such that LMI (14) holds for $i = 1, 2, \ldots, N$ iff the LMI (15) holds for both maximum and minimum eigenvalues of $(\mathcal{L}+\mathcal{P})$. Hence, LMI (15) does not depend on number of followers in a platoon and is scaled with individual vehicles. The LMI (15) is the relaxed form of (14) to facilitate its solution as reported in [9], [41].

B. Internal Stability Analysis for Vehicle Platooning Under Random Consecutive Packet Drop

Internal stability in terms of a stability margin can be measured by the absolute value of the least stable closed-loop pole or eigenvalue in the discrete time domain. Therefore, the following Theorem applies to analysing the effect of *(i)* packet drop and *(ii)* number of vehicle platoon members on the stability margin of vehicle platoon systems with both BPF and BPLF topologies in the discrete time domain.

Theorem 3: If given discrete time closed-loop system (16), shown at the bottom of the next page, where (17), shown at the bottom of the next page, is the characteristic polynomial of (16), with independent variable z, non-zero constant real number $\{K_s, K_v, K_a, \tau, T_s\}$, mean packet drop rate r, consecutive packet drop $\delta_{max} = \delta$ and eigenvalue $\lambda_i = \lambda_i(\mathcal{L}+\mathcal{P})$, $i = 1, 2, \ldots, N$, is asymptotically stable $\forall\lambda_i = \lambda_i(\mathcal{L}+\mathcal{P})$, $i = 1, 2, \ldots, N$, the following statements hold:

3.1) closed-loop system (13) is asymptotically stable.

3.2) If λ_i goes to zero then (17) has three characteristic roots approaching zero and the others have certain value not approaching zero.

3.3) No characteristic root of (17) will be zero unless λ_i goes to zero.

The analytical proof of Theorem 3 is presented in the Appendix.

From the Theorem 3, following remarks can be drawn.

Remarks 2.

- Eqn. (17) is the characteristic polynomial of i^{th} vehicle of a homogeneous vehicle platoon system with undirected topologies (i.e. BPF and BPLF topology) and external disturbance under multiple consecutive packet drops modelled as in (9)-(10) with mean packet drop rate r. Closed-loop system (13) is said to be asymptotically stable if all the characteristic roots of (17) are within a unit circle, i.e., $|z| < 1$ $\forall\lambda_i = \lambda_i(\mathcal{L}+\mathcal{P}), i = 1, 2, \ldots, N$. It can also be inferred that closed-loop system (13) is asymptotically stable if all the characteristic roots of (17) are $|z| < 1$ for both minimum and maximum eigenvalues of $(\mathcal{L}+\mathcal{P})$. Therefore, if the absolute value of the least stable eigenvalue of (17) is within a unit circle for both minimum and maximum eigenvalues of $(\mathcal{L}+\mathcal{P})$ then closed-loop system (13) is internally stable.
- If λ_i goes to zero, then characteristic roots of (17) will be independent of the value of controller gains and mean packet drop rate $\{K_s, K_v, K_a, r\}$ and will only depend on the choice of sampling time and time constant of the power train $\{T_s, \tau\}$. However, the nature of these roots can be analysed from the property of discriminant which is not within the scope of this paper.

Theorem 3 provides an idea of the asymptotic stability of the closed-loop system (13), which is a function of eigenvalue of undirected topologies. Next, this paper investigates the internal stability of the closed-loop system as a function of follower vehicles in a homogenous platoon with BPF and

$$\boldsymbol{\Pi} = \begin{bmatrix} \boldsymbol{\Xi} - \boldsymbol{\Theta} - \bar{\boldsymbol{P}} & * & * & * & * & * \\ \boldsymbol{\Theta} & -\boldsymbol{\Xi} - \boldsymbol{\Theta} & * & * & * & * \\ \boldsymbol{0} & \boldsymbol{0} & -\gamma^2 \boldsymbol{I}_N & * & * & * \\ ((\boldsymbol{I}_N \otimes \boldsymbol{A}_d)\bar{\boldsymbol{P}} + \tilde{\boldsymbol{L}}(1-r) \otimes \boldsymbol{B}_d \boldsymbol{Z}) & \tilde{\boldsymbol{L}} r \otimes \boldsymbol{B}_d \boldsymbol{Z} & \boldsymbol{I}_N \otimes \boldsymbol{B}_d & -\bar{\boldsymbol{P}} & * & * \\ \delta_{max}((\boldsymbol{I}_N \otimes \boldsymbol{A}_d)\bar{\boldsymbol{P}} + \tilde{\boldsymbol{L}}(1-r) \otimes \boldsymbol{B}_d \boldsymbol{Z} - \bar{\boldsymbol{P}}) & \delta_{max}(\tilde{\boldsymbol{L}} r \otimes \boldsymbol{B}_d \boldsymbol{Z}) & \delta_{max}(\boldsymbol{I}_N \otimes \boldsymbol{B}_d) & \boldsymbol{0} & -\delta_{max}\bar{\boldsymbol{R}} & * \\ (\boldsymbol{I}_N \otimes \boldsymbol{C})\bar{\boldsymbol{P}} & \boldsymbol{0} & \boldsymbol{0} & \boldsymbol{0} & \boldsymbol{0} & -\boldsymbol{I}_N \end{bmatrix} < \boldsymbol{0}. \tag{14}$$

$$\tilde{\boldsymbol{\Pi}}_i = \begin{bmatrix} \boldsymbol{\Xi}_0 - \boldsymbol{\Theta}_0 - \bar{\boldsymbol{P}}_0 & * & * & * & * & * \\ \boldsymbol{\Theta}_0 & -\boldsymbol{\Xi}_0 - \boldsymbol{\Theta}_0 & * & * & * & * \\ \boldsymbol{0} & \boldsymbol{0} & -\gamma^2 \boldsymbol{I}_1 & * & * & * \\ (\boldsymbol{A}_d \bar{\boldsymbol{P}}_0 + \lambda_i(1-r)\boldsymbol{B}_d \boldsymbol{Z}) & \lambda_i r \boldsymbol{B}_d \boldsymbol{Z} & \boldsymbol{B}_d & -\bar{\boldsymbol{P}}_0 & * & * \\ \delta_{max}(\boldsymbol{A}_d \bar{\boldsymbol{P}}_0 + \lambda_i(1-r)\boldsymbol{B}_d \boldsymbol{Z} - \bar{\boldsymbol{P}}_0) & \delta_{max}(\lambda_i r \boldsymbol{B}_d \boldsymbol{Z}) & \delta_{max}\boldsymbol{B}_d & \boldsymbol{0} & -\delta_{max}\bar{\boldsymbol{R}}_0 & * \\ \boldsymbol{C}\bar{\boldsymbol{P}}_0 & \boldsymbol{0} & \boldsymbol{0} & \boldsymbol{0} & \boldsymbol{0} & -\boldsymbol{I}_1 \end{bmatrix} < \boldsymbol{0}. \tag{15}$$

BPLF topologies, respectively, under consecutive packet drops with mean packet drop rate r.

Theorem 4: The closed-loop system (13) with BPF topology is asymptotically stable if two given characteristic polynomials (18) and (19), shown at the bottom of the next page, with independent variable z, non-zero constant real number $\{K_s, K_v, K_a, \tau, T_s\}$, mean packet drop rate r and number of follower vehicle (N) are asymptotically stable $\forall i = 1, 2, \ldots, N$. Here, $\{\lambda^\star_{min}, \lambda^\star_{max}\}$ represent minimum and maximum eigenvalues of $(\mathcal{L}_{BPF} + \mathcal{P}_{BPF})$.

Theorem 5: The closed-loop system (13) with BPLF topology is asymptotically stable if two given characteristic polynomials (20) and (21), shown at the bottom of the next page, are asymptotically stable with independent variable z, non-zero constant real number $\{K_s, K_v, K_a, \tau, T_s\}$, mean packet drop rate r and number of follower vehicle (N) $\forall i = 1, 2, \ldots, N$. Here, $\{\lambda^\dagger_{min}, \lambda^\dagger_{max}\}$ represent minimum and maximum eigenvalues of $(\mathcal{L}_{BPLF} + \mathcal{P}_{BPLF})$.

The analytical proof of the Theorem 4 and 5 are presented in the Appendix.

From the Theorem 4 and 5, following remarks can be drawn.

Remarks 3.

- When minimum and maximum eigenvalue $(\lambda_{min}, \lambda_{max})$ are used, $\nabla^\star_{min}(z, \lambda^\star_{min})$, $\nabla^\star_{max}(z, \lambda^\star_{max})$ in (18), (19), $\nabla^\dagger_{min}(z, \lambda^\dagger_{min})$, $\nabla^\dagger_{max}(z, \lambda^\dagger_{max})$ in (20), (21) represent two characteristic polynomials of i^{th} vehicle of a homogeneous vehicle platoon system with BPF and BPLF topology under consecutive packet drop modelled as in (10) with mean packet drop rate r and external disturbance, respectively.
- $\{\nabla^\star_{min}(z, \lambda^\star_{min}), \nabla^\star_{max}(z, \lambda^\star_{max})\}$ in (18), (19), $\{\nabla^\dagger_{min}(z, \lambda^\dagger_{min}), \nabla^\dagger_{max}(z, \lambda^\dagger_{max})\}$ in (20), (21) are obtained from (17) using eigenvalues $\{\lambda_{min}(\mathcal{L}_{BPF} + \mathcal{P}_{BPF}), \lambda_{max}(\mathcal{L}_{BPF} + \mathcal{P}_{BPF})\}$ and $\{\lambda_{min}(\mathcal{L}_{BPLF} + \mathcal{P}_{BPLF}), \lambda_{max}(\mathcal{L}_{BPLF} + \mathcal{P}_{BPLF})\}$, respectively. Since, the eigenvalues $\lambda_i(\mathcal{L}_{BPF} + \mathcal{P}_{BPF})$ and $\lambda_i(\mathcal{L}_{BPLF} + \mathcal{P}_{BPLF})$ will be varying towards both lower and upper bound with the increasing number of platoon followers (N), thus, all the characteristic roots in (18)-(21) will be depending on N and hence, internal stability of (13) will be affected by N. It is noted that the smallest eigenvalue of BPLF topology is one [6].
- Only, characteristic roots under BPF topology, i.e., $\nabla^\star_{min}(z, \lambda^\star_{min})$ in (18) are depending on the sampling time and time constant of power train $\{T_s, \tau\}$ for large N. Whereas, including $\{T_s, \tau\}$, the characteristic roots of $\nabla^\star_{max}(z, \lambda^\star_{max})$ in (19) and $\nabla^\dagger_{min}(z, \lambda^\dagger_{min})$, $\nabla^\dagger_{max}(z, \lambda^\dagger_{max})$ in (20), (21) are also depending on the other parameters such as controller gains and mean packet drop rate $\{K_s, K_v, K_a, r\}$ even if N is large. Since, τ is constant, therefore, selection of appropriate T_s is important when N is large for the platoon control systems with BPF and BPLF topologies under external disturbances and random consecutive packet drop.

IV. Numerical and Simulation Results

The effectiveness of the proposed methodology for achieving internal stability and cooperative motion of homogeneous vehicle platoon systems is evaluated for two different undirected network topologies, i.e., BPF and BPLF and different numbers of follower vehicles under random consecutive packet drop with different packet drop rates. A desired spacing $d_{i,i-1} = 25$ m is selected among the vehicles in a platoon [7]. It is assumed that for all the homogeneous followers there is no collision at initial time $t = 0$ s and the initial states are random in nature. The power train time constant is selected as $\tau = 0.5$ s [7]. The leader's speed is considered constant at 72 km h^{-1} [9], [10], [14]. The continuous time system is discretised with specified sampling time $T_s = 0.1$ s [9], [14] for designing the controller. Furthermore, an $\mathcal{L}_2$ norm bounded the external disturbance input, i.e., $\mathbb{E}\{\| w_i(k) \|_{\mathcal{L}_2}\} < +\infty$ to the acceleration of all followers is considered as a unity amplitude square wave. The starting period of the external disturbances is at $t = 100$ s with a duration of $t = 5$ s. The robustness measures, γ, of the closed-loop platoon system under random packet drop can be defined as $\gamma \geq \sup \frac{\mathbb{E}\{\| \boldsymbol{Y} \|_{L_2}\}}{\mathbb{E}\{\| \boldsymbol{W} \|_{L_2}\}}$ which describes the sensitivity or attenuation effect of the energy of external disturbances on the output tracking error [9], [48]–[50]. To obtain controller gain by minimising the squared value of robustness measures, i.e., γ^2 using the LMI (15), the following optimisation problem can be computed by YALMIP toolbox [51] combining with the SeDuMi solver [52] in MATLAB environment:

$$\begin{aligned} &\min_{\bar{\boldsymbol{P}}_0, \bar{\boldsymbol{Q}}_0, \bar{\boldsymbol{R}}_0, \boldsymbol{\Xi}_0, \boldsymbol{\Theta}_0, \boldsymbol{Z}, \gamma} \gamma \quad . \\ &s.t. (15) \end{aligned} \tag{22}$$

$$\begin{aligned} G_i(z) = {} & {T_s}^3 z^\delta [(\tau z^{\delta+3} + (T_s - 3\tau) z^{\delta+2} + (3\tau - 2T_s) z^{\delta+1} + (T_s - \tau) z^\delta) + \lambda_i ((K_a - K_v T_s + K_s {T_s}^2) T_s r - (2K_a - K_v T_s) \\ & \times T_s r z + K_a T_s r z^2 + (K_a - K_v T_s + K_s {T_s}^2) T_s (1-r) z^\delta + (K_v T_s - 2K_a) T_s (1-r) z^{\delta+1} + K_a T_s (1-r) z^{\delta+2})]^{-1}, \\ & \forall i = 1, 2, \ldots, N \end{aligned} \tag{16}$$

$$\begin{aligned} \nabla_i(z, \lambda_i) = {} & [(\tau z^{\delta+3} + (T_s - 3\tau) z^{\delta+2} + (3\tau - 2T_s) z^{\delta+1} + (T_s - \tau) z^\delta) + \lambda_i ((K_a - K_v T_s + K_s {T_s}^2) T_s r - (2K_a - K_v T_s) \\ & \times T_s r z + K_a T_s r z^2 + (K_a - K_v T_s + K_s {T_s}^2) T_s (1-r) z^\delta + (K_v T_s - 2K_a) T_s (1-r) z^{\delta+1} + K_a T_s (1-r) z^{\delta+2})], \\ & \forall i = 1, 2, \ldots, N \end{aligned} \tag{17}$$

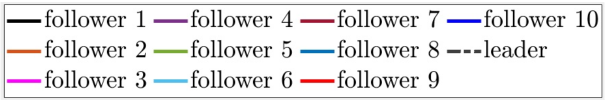

Fig. 1. Legend for Figs. 2 to 4.

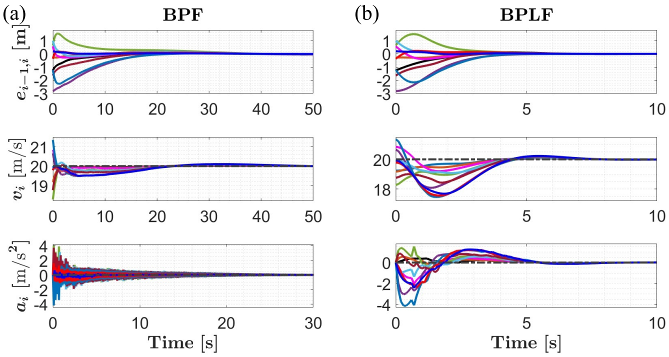

Fig. 2. Transient response of 10 follower vehicles' states (see colour legend in Fig. 1) in a platoon with (a) BPF (left panel) and (b) BPLF (right panel) topologies under 6 consecutive packet drop with 30% packet drop rate before action of external disturbances.

A. Time Response Analysis

The transient responses of 10 follower vehicle's states, i.e., inter-vehicular distance error ($e_{i,i-1}(k) = s_i(k) - s_{i-1}(k) - d_{i,i-1}$) among the consecutive follower, velocity (v_i) and acceleration (a_i) in a vehicle platoon system are depicted in Figs. 1 to 4 using the designed controller to achieve control objectives (7) under random consecutive packet drops and external distubance, where Fig. 1 represents the legend of Figs. 2 to 4. These transient responses are compared for a vehicle platoon system with two different network topologies, i.e., BPF and BPLF under $\delta_{max} = \delta = 6$ consecutive packet drops with 30% packet drop rate and external disturbances. By solving the LMI (15) using (22) and $T_s = 0.1$ s, the controller gains are obtained for BPF and BPLF topology as $\boldsymbol{K}_{BPF} = -[0.7205, 5.3906, 2.5159]$ and $\boldsymbol{K}_{BPLF} = -[0.8843, 1.6439, 0.6259]$, respectively. It is assumed that at time instant $t = 0$ s, the follower states are mismatched, e.g., up-to 3 m inter vehicular distance error ($e_{i,i-1}$) among the consecutive platoon members which describes the variation in velocities (v_i) of the followers. Fig. 2 describes the transient responses of follower's states, i.e., ($e_{i,i-1}, v_i$) and acceleration (a_i), before applying external disturbances. From Fig. 2, it can be observed that the dynamics of all follower vehicles are converging to desired behaviours such as maintaining zero inter-vehicular distance error, matching to leader's velocity (i.e., 20 m s^{-1} which is constant) and zero accelerations (a_i), when the controllers are activated. The converging time of all the follower states in the BPF topology is higher than the converging time of follower states in the BPLF topology under 6 consecutive packet drop with 30% packet drop rate since the leader vehicle is connected to all the followers in BPLF topology, as is consistent with [9], [14], since all the followers receive information directly from the leader vehicle when the vehicle platoon is in a BPLF topology. Fig. 3 compares the behaviour of follower's states when the external disturbance is applied to each follower and network imperfections are introduced into the vehicle platoon system for both BPF and BPLF topologies. Under such scenarios, the inter-vehicular distance error (maximum 4.9 m), settling time, and velocity amplification is higher for BPF topology as compared to BPLF topology where maximum inter-vehicular distance error is 1.3 m. For BPLF topology the inter-vehicular distance error exists only for the first follower; other followers are maintaining almost zero error. This is due to the fact that all the followers are pinned to the leader, thus maintaining

$$\nabla^{\star}_{min}(z, \lambda^{\star}_{min}) = [(\tau z^{\delta+3} + (T_s - 3\tau)z^{\delta+2} + (3\tau - 2T_s)z^{\delta+1} + (T_s - \tau)z^{\delta}) + (1/N^2)((K_a - K_v T_s + K_s T_s{}^2)T_s r - (2K_a - K_v T_s)T_s r z + K_a T_s r z^2 + (K_a - K_v T_s + K_s T_s{}^2)T_s(1-r)z^{\delta} + (K_v T_s - 2K_a)T_s(1-r)z^{\delta+1} + K_a T_s(1-r)z^{\delta+2})], \tag{18}$$

$$\nabla^{\star}_{max}(z, \lambda^{\star}_{max}) = [(\tau z^{\delta+3} + (T_s - 3\tau)z^{\delta+2} + (3\tau - 2T_s)z^{\delta+1} + (T_s - \tau)z^{\delta}) + 4((K_a - K_v T_s + K_s T_s{}^2)T_s r - (2K_a - K_v T_s)T_s r z + K_a T_s r z^2 + (K_a - K_v T_s + K_s T_s{}^2)T_s(1-r)z^{\delta} + (K_v T_s - 2K_a)T_s(1-r)z^{\delta+1} + K_a T_s(1-r)z^{\delta+2})], \tag{19}$$

$$\nabla^{\dagger}_{min}(z, \lambda^{\dagger}_{min}) = [(\tau z^{\delta+3} + (T_s - 3\tau)z^{\delta+2} + (3\tau - 2T_s)z^{\delta+1} + (T_s - \tau)z^{\delta}) + ((K_a - K_v T_s + K_s T_s{}^2)T_s r - (2K_a - K_v T_s)T_s r z + K_a T_s r z^2 + (K_a - K_v T_s + K_s T_s{}^2)T_s(1-r)z^{\delta} + (K_v T_s - 2K_a)T_s(1-r)z^{\delta+1} + K_a T_s(1-r)z^{\delta+2})], \tag{20}$$

$$\nabla^{\dagger}_{max}(z, \lambda^{\dagger}_{max}) = [(\tau z^{\delta+3} + (T_s - 3\tau)z^{\delta+2} + (3\tau - 2T_s)z^{\delta+1} + (T_s - \tau)z^{\delta}) + 5((K_a - K_v T_s + K_s T_s{}^2)T_s r - (2K_a - K_v T_s)T_s r z + K_a T_s r z^2 + (K_a - K_v T_s + K_s T_s{}^2)T_s(1-r)z^{\delta} + (K_v T_s - 2K_a)T_s(1-r)z^{\delta+1} + K_a T_s(1-r)z^{\delta+2})], \tag{21}$$

This article has been accepted for inclusion in a future issue of this journal. Content is final as presented, with the exception of pagination.

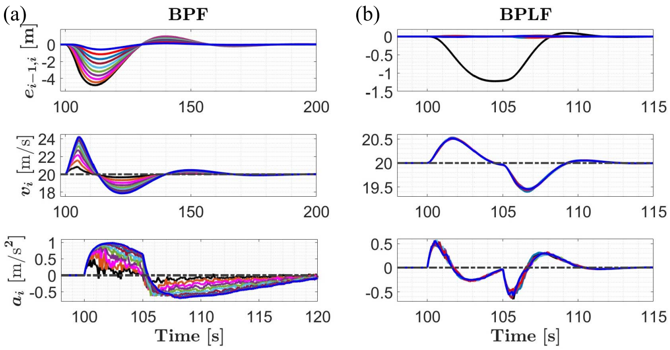

Fig. 3. Transient response of 10 followers' states (see colour legend in Fig. 1) under external disturbance and 6 consecutive packet drop with 30% packet drop rate for (a) BPF (left panel) and (b) BPLF (right panel) topologies.

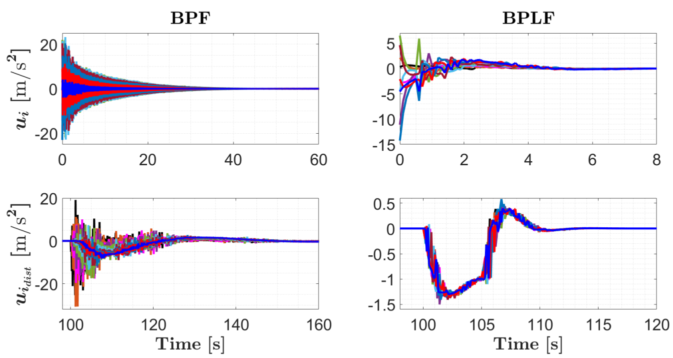

Fig. 4. Control signal to the 10 followers (see colour legend in Fig. 1) during the initial transient (upper panel) and after action of external disturbances (lower panel) under 6 consecutive packet drop with 30% packet drop rate.

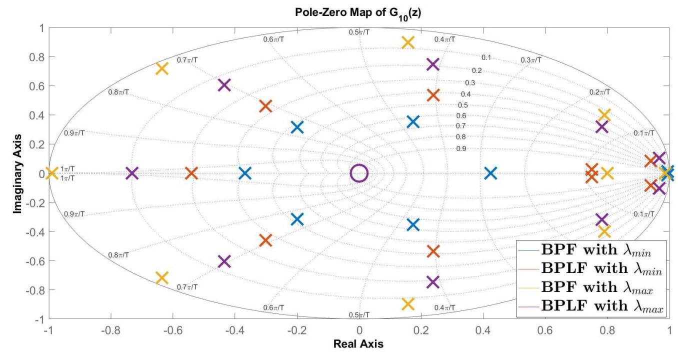

Fig. 5. Closed-loop pole and zero (i.e., 'x' and 'o', respectively) plot for vehicle platoon system (16) with both $\{\lambda_{min}(\mathcal{L}_{BPF}+\mathcal{P}_{BPF}), \lambda_{min}(\mathcal{L}_{BPLF}+\mathcal{P}_{BPLF})\}$ and $\{\lambda_{max}(\mathcal{L}_{BPF}+\mathcal{P}_{BPF}), \lambda_{max}(\mathcal{L}_{BPLF}+\mathcal{P}_{BPLF})\}$ where $\{N=10, T_s=0.1\text{s}, r=0.3, \delta_{max}=6\}$.

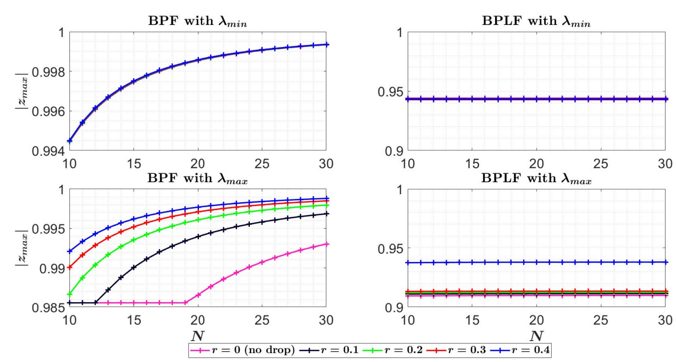

Fig. 6. Scaling trend of stability margin, i.e., $|z_{max}|$ with varying number of followers ($N=10$ to 30) and packet drop rate ($r=0, 0.1, 0.2, 0.3, 0.4$) for a vehicle platoon system with BPF and BPLF topology when $\{T_s = 0.1\text{s}, \delta_{max}=6\}$.

the same dynamic evolution [6], [9]. It is also noted that each follower vehicle has maintained almost the same velocity and acceleration under the BPLF topology. Fig. 4 depicts all the control inputs converging to zero for both BPF and BPLF topologies before and after activating external disturbances to each follower. Highly oscillatory control inputs for the BPF topology describe the requirement of high control effort as compared to the BPLF topology under random consecutive packet drop.

B. Internal Stability Analysis

To demonstrate the effect of two network topologies, number of platoon followers, random consecutive packet drop with varying packet drop rate and sampling time on the internal stability of vehicle platoon system, the variation on stability margin, measured by absolute value of least stable closed-loop pole location in discrete time, i.e., z-plane, is investigated. Fig. 5 shows the closed-loop pole and zero location of $i = 10^{th}$ vechicle using (16) when a vehicle platoon system (13) with 10 followers and both BPF and BPLF topologies, under 6 consecutive packet drops with 30% packet drop rate, $T_s = 0.1$ s and the designed controller in the frequency domain using MATLAB *'pzmap'* command. Fig. 5 shows that all the closed-loop zeros are on the centre of the unit circle and all poles are within the unit circle for both topologies, but the closed-loop poles are shifting more towards high frequency and low damping when BPF topology is used, compared to BPLF topology, which defines the degradation of stability as reported in [53]. Therefore, Fig. 5 indicates that when the leader is connected with all follower vehicles, i.e., under BPLF topology, both internal stability and robustness are improving as compared to BPF topology where only first follower is connected with the leader vehicle. It is noteworthy that in a platoon of N vehicles, the most stringent conditions for stability lie on the N^{th} vehicle since $\lambda_{\min}$ and λ_{max} for both BPF and BPLF topologies approach the lower and upper limit, respectively for the N^{th} vehicle. Consequently, if the closed-loop stability is achieved for the N^{th} vehicle the control law also ensures stability for the remaining vehicles in the platoon. Therefore, for the aforementioned analysis, the stability of the N^{th} vehicle in the platoon, i.e., $N = 10$ is considered.

Next, to demonstrate the stability margin and its variation (i.e., scaling trend) we consider different numbers of platoon members ($N = 10$ to 30) for the two different network topologies (i.e., BPF and BPLF), varying packet drop rate ($r = 0$ to 0.4965, i.e., no drop to 49.65%) with fixed number of consecutive packet drop, i.e., $\delta_{max} = 6$, $T_s = 0.1$ s and designed controller gain (as presented in the previous subsection). Fig. 6 compares the scaling trend of the absolute

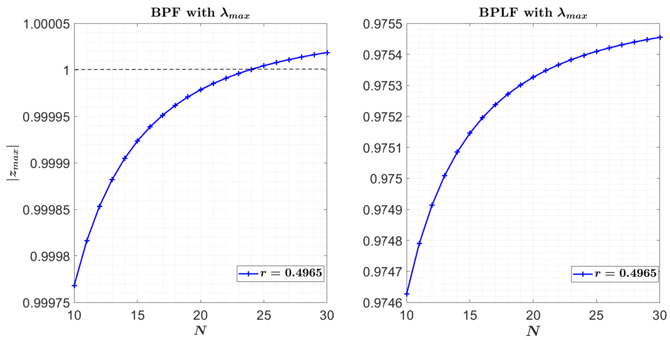

Fig. 7. Scaling trend of stability margin, i.e., $|z_{max}|$ with varying number of followers ($N = 10$ to 30) and 49.65% packet drop rate ($r = 0.4965$) for a vehicle platoon system with BPF and BPLF topology when $\{T_s = 0.1\text{s}, \delta_{max} = 6\}$.

least stable closed-loop eigenvalue, represented by $|z_{max}|$, with varying N and packet drop rate r for both maximum and minimum $\{\lambda_{max}(\mathcal{L}_{BPF} + \mathcal{P}_{BPF}), \lambda_{max}(\mathcal{L}_{BPLF} + \mathcal{P}_{BPLF})\}$ and $\{\lambda_{min}(\mathcal{L}_{BPF} + \mathcal{P}_{BPF}), \lambda_{min}(\mathcal{L}_{BPLF} + \mathcal{P}_{BPLF})\}$ of BPF and BPLF topology using (16), respectively. In Figs. 6 and 7, the stability margin, represented by $|z_{max}|$, is moving towards unit circle boundary, i.e., $|z| = 1$ which indicates $|z_{max}|$ is moving towards high frequency and low damping when both number of follower vehicle (N) and packet drop rate (r) are increasing. Fig. 6 describes the scaling trend of stability margin ($|z_{max}|$) with both $\{\lambda_{min}, \lambda_{max}\}$ of BPF and BPLF topology when N is varying from 10 to 30 and r is varying from 0 to 0.4 (r = no drop to 40%). It is seen from Fig. 6 that scaling trends of ($|z_{max}|$) are almost unaltered with the chosen N and r when λ_{min} is used for both BPF and BPLF topologies. Whereas, scaling trend of ($|z_{max}|$) is shifting towards unit circle boundary, i.e., $|z| = 1$ when both N and r are increasing with λ_{max} of both BPF and BPLF topologies. Also, degradation of internal stability under BPF topology is higher, since $|z_{max}|$ under BPF topology is approaching towards unit circle boundary more quickly with increasing N and r as compared to BPLF.

Since variation of stability margin, $|z_{max}|$, is higher with higher N and r when λ_{max} is used for both topologies, we assess the variation of $|z_{max}|$ with higher packet drop rate ($r = 0.4965$), and $N = 10$ to 30 when λ_{max} of BPF and BPLF topologies are used as shown in Fig. 7. This assessment is to obtain the maximum allowable r and N for a platoon control system to be internally stable (i.e., $|z| < 1$) by maintaining cooperative motion (i.e., specified inter-vehicular distance, desired speed) with both BPF and BPLF topologies while controller is designed at specified parameter values, i.e., at $\{N = 10, T_s = 0.1\text{ s}, \delta_{max} = 6, r = 0.3\}$. Fig. 7 shows that a platoon control system with BPF topology controlled by the designed controller ensures internal stability and can maintain cooperative motion for a maximum $N = 24$ follower vehicles under 6 consecutive packet drop with 49.65% packet drop rate (i.e., $r = 0.4965$). This is because $|z_{max}| > 1$ when $N \geq 25$ in a platoon with BPF topology under $\{\delta_{max} = 6, r = 0.4965\}$. However, a platoon control system with BPLF topology controlled by the designed controller allows $N > 30$ and $r > 0.4965$. Therefore, a controller designed

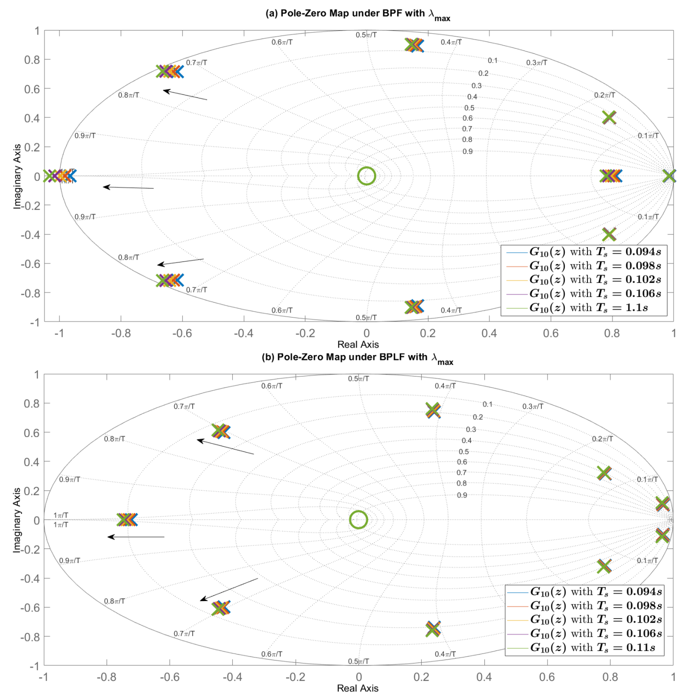

Fig. 8. Variation of closed-loop pole/zero (i.e., x/o) for vehicle platoon system (16) with $N = 10$, two network topologies and varying sampling time (T_s) under $\delta_{max} = 6$ consecutive packet drop with 30% packet drop rate (a) BPF (b) BPLF.

using the proposed methodology with a fixed $\{N, T_s, \delta_{max}, r\}$ for a vehicle platoon control system is more robust and is ensures higher internal stability against maximum allowable packet drop rate and number of follower vehicles when BPLF topology is preferred to BPF topology. It is to be noted that the internal stability analysis with the eqns. (18)-(21) are not separately presented here for the sake of brevity. In addition to the above analysis, the variation of closed-loop poles and zeros of (16) with varying sampling time (T_s) is also important for internal stability and performance analysis of such kinds of networked control systems [54]. Therefore, to demonstrate the robustness of the platoon control system (13) controlled by the designed controller at $\{N = 10, T_s = 0.1\text{ s}, \delta_{max} = 6, r = 0.3\}$ against the varying $T_s = 0.094$ s, 0.098 s, 0.102 s, 0.106 s, 0.11 s, this paper analyses closed-loop stability using λ_{max} of both BPF and BPLF topologies and $\{N = 10, \delta_{max} = 6, r = 0.3\}$ by pole-zero plot, as shown in Fig. 8 (a) and Fig. 8 (b), respectively, in discrete time. In Fig. 8, it is seen that the closed-loop poles are moving towards high frequency and low damping when T_s is increasing for system (16) at $N = 10$ with both BPF and BPLF topologies, thus, both stability and performances are degrading [44], [53]. The closed-loop poles are moving faster towards high frequency and low damping as T_s is increasing when BPF topology is used as compared to BPLF topology. Also, closed-loop system (13) with BPF topology is becoming unstable ($|z_{max}| > 1$) when $T_s = 0.106$ s, while closed-loop system (13) with BPLF topology is stable (i.e., $|z| < 1$) for this T_s. Therefore, it can be inferred that the designed platoon control system with BPLF topology, under multiple consecutive packet drops and external disturbance, is more robust and internally stable against sampling time

(T_s) compared to BPF topology. However, investigation on other platoon control parameters such as variation in separation distance amongst the member vehicles ensuring safety may be another interesting research problem to improve internal stability and robustness of a platoon control system under network imperfections that will be explored in future.

V. Conclusion

In this paper, an LMI based distributed controller satisfying bounded H_∞ norm has been designed for vehicle platoons under random multiple consecutive packet drops and external disturbance. Stability margin analysis has been used to understand internal stability with respect to two different undirected network topologies and platoon size under random consecutive packet drop with varying packet drop rates and external disturbances. The designed controller has been tested in a MATLAB simulation platform in terms of the time domain transient response for a vehicle platoon system with 10 follower vehicles considering two different network topologies, BPF and BPLF, under aforementioned scenarios. Simulation results demonstrate the effectiveness of the proposed controller for maintaining vehicle platooning stability under random consecutive packet drop and external disturbances while ensuring specified inter-vehicular distance. From the analysis of the proposed method, it is shown that both the stability and robustness of the vehicle platoon is better when the leader is connected to all the followers, i.e., for a BPLF topology as compared to a BPF topology. As a scope of future work, the proposed method can be extended to address various parameters such as directed topology, CTHP, time varying delay, parametric uncertainty, and asymmetric packet drop in the communication network and switching between topologies for both homogeneous and heterogeneous vehicle platoon systems.

Appendix

This section describes the systematic proof of all Theorems that use the tracking error dynamic model of the homogenous vehicle platoon to establish the stability criteria and design an identical distributed controller based on Lyapunov-Krasovskii theory. First we derive the model of closed-loop error dynamics and subsequently using Lyapunov-Krasovskii function, Theorem 1 in Section III is proved for a platoon of vehicles.

A. Closed-Loop Dynamics and Its Transfer Function Under Random Consecutive Packet Drop

Since, the packet drop is modelled as a Bernoulli probabilistic distribution as in (2), the expected value of the closed-loop tracking error dynamics under random consecutive packet drop modelled as (10) with (2) can be represented after applying the expectation value to the closed-loop system (13) as:

$$\begin{aligned}\mathbb{E}(\boldsymbol{X}(k+1)) &= ((\boldsymbol{I}_N \otimes \boldsymbol{A}_d) + ((\mathcal{L}+\mathcal{P})(1-r) \otimes \boldsymbol{B}_d\boldsymbol{K}))\\ &\quad \times \mathbb{E}(\boldsymbol{X}(k)) + ((\mathcal{L}+\mathcal{P})r \otimes \boldsymbol{B}_d\boldsymbol{K})\mathbb{E}(\boldsymbol{X}(k-\beta_k))\\ &\quad + (\boldsymbol{I}_N \otimes \boldsymbol{B}_d)\mathbb{E}(\boldsymbol{W}(k)),\\ \mathbb{E}(\boldsymbol{Y}(k)) &= (\boldsymbol{I}_N \otimes \boldsymbol{C})\mathbb{E}(\boldsymbol{X}(k)). \end{aligned} \tag{23}$$

Now, define $\bar{\boldsymbol{\Gamma}}(k) = [\boldsymbol{\Gamma}_1^T(k), \boldsymbol{\Gamma}_2^T(k), \ldots, \boldsymbol{\Gamma}_{\beta_k}^T(k)]^T = [\boldsymbol{X}^T(k-1), \boldsymbol{X}^T(k-2), \ldots, \boldsymbol{X}^T(k-\beta_k)]^T$ where, $\boldsymbol{\Gamma}_l(k) = \boldsymbol{X}(k-l), \forall l = 1, 2, \ldots, \beta_k$ and the augmented state $\tilde{\boldsymbol{X}}(k) = [\boldsymbol{X}^T(k), \bar{\boldsymbol{\Gamma}}^T(k)]^T$. The eqn. (23) can be re-written in the form of expected value as (24), shown at the bottom of the next page. Similar to [9], the discrete time transfer function from $\mathbb{E}(\boldsymbol{W}(k))$ to $\mathbb{E}(\boldsymbol{Y}(k))$ of (24) by assuming zero initial tracking error can be obtained as (25), shown at the bottom of the next page, with $\beta_k = \delta$. Now, using the system (23), the proof of Theorem 1 is described below.

B. Proof of Theorem 1

Define the Lyapunov-Krasovskii function candidate with $\boldsymbol{P} = \boldsymbol{P}^T > \boldsymbol{0}$, $\boldsymbol{Q} = \boldsymbol{Q}^T > \boldsymbol{0}$, and $\boldsymbol{R} = \boldsymbol{R}^T > \boldsymbol{0}$ as:

$$\begin{aligned}V(k) &= V_1(k) + V_2(k) + V_3(k) = \boldsymbol{X}^T(k)\boldsymbol{P}\boldsymbol{X}(k)\\ &\quad + \sum_{i=k-\beta_k}^{k-1} \boldsymbol{X}^T(i)\boldsymbol{Q}\boldsymbol{X}(i)\\ &\quad + \sum_{j=-\delta_{max}}^{-1}\sum_{j=k+i}^{k-1} \Delta\boldsymbol{X}^T(j)\boldsymbol{R}\Delta\boldsymbol{X}(j), \end{aligned} \tag{26}$$

where, $V_1(k) = \boldsymbol{X}^T(k)\boldsymbol{P}\boldsymbol{X}(k)$, $V_2(k) = \sum_{i=k-\beta_k}^{k-1} \boldsymbol{X}^T(i)\boldsymbol{Q}\boldsymbol{X}(i)$ and $V_3(k) = \sum_{j=-\delta_{max}}^{-1}\sum_{j=k+i}^{k-1} \Delta\boldsymbol{X}^T(j)\boldsymbol{R}\Delta\boldsymbol{X}(j)$.

The expected value of the inequality satisfying H_∞ norm bound $\gamma > 0$ can be represented as [9], [48]:

$$\mathbb{E}(\Delta V(k)) + \mathbb{E}(\boldsymbol{Y}^T(k)\boldsymbol{Y}(k) - \gamma^2\boldsymbol{W}^T(k)\boldsymbol{W}(k)) < \boldsymbol{0}, \tag{27}$$

where, $\Delta V(k) = V(k+1) - V(k)$.

Using (26),

$$\begin{aligned}\mathbb{E}(\Delta V_1(k)) &= \mathbb{E}(V_1(k+1) - V_1(k))\\ &= \mathbb{E}(\boldsymbol{X}^T(k+1)\boldsymbol{P}\boldsymbol{X}(k+1) - \boldsymbol{X}^T(k)\boldsymbol{P}\boldsymbol{X}(k)). \end{aligned} \tag{28}$$

Using (23) in (28) and assuming $\bar{\boldsymbol{A}}_d = ((\boldsymbol{I}_N \otimes \boldsymbol{A}_d) + (\mathcal{L}+\mathcal{P})(1-r) \otimes \boldsymbol{B}_d\boldsymbol{K})$, $\tilde{\boldsymbol{L}} = (\mathcal{L}+\mathcal{P})$, and augmented state $\boldsymbol{\eta}(k) = \left[\boldsymbol{X}^T(k)\ \boldsymbol{X}^T(k-\beta_k)\ \boldsymbol{W}^T(k)\right]^T$, the expected value of $\Delta V_1(k)$ i.e. $\mathbb{E}(\Delta V_1(k))$ can be written as (29), shown at the bottom of the next page. Similarly using (26), $\mathbb{E}(\Delta V_2(k)) = \mathbb{E}(V_2(k+1) - V_2(k)) = \mathbb{E}(\sum_{i=k+1-\beta_k}^{k} \boldsymbol{X}^T(i)\boldsymbol{Q}\boldsymbol{X}(i) - \sum_{i=k-\beta_k}^{k-1} \boldsymbol{X}^T(i)\boldsymbol{Q}\boldsymbol{X}(i)) =$

$$\mathbb{E}[\boldsymbol{\eta}^T(K)]\begin{bmatrix}\boldsymbol{Q} & \boldsymbol{0} & \boldsymbol{0}\\ * & -\boldsymbol{Q} & \boldsymbol{0}\\ * & * & \boldsymbol{0}\end{bmatrix}\mathbb{E}[\boldsymbol{\eta}(K)], \tag{30}$$

and,

$$\begin{aligned}\mathbb{E}(\Delta V_3(k)) &= \mathbb{E}(V_3(k+1) - V_3(k))\\ &= \mathbb{E}(\sum_{i=-\delta_{max}}^{-1}\sum_{j=k+1+i}^{k} \Delta\boldsymbol{X}^T(j)\boldsymbol{R}\Delta\boldsymbol{X}(j)\\ &\quad - \sum_{i=-\delta_{max}}^{-1}\sum_{j=k+i}^{k-1} \Delta\boldsymbol{X}^T(j)\boldsymbol{R}\Delta\boldsymbol{X}(j))\\ &= \mathbb{E}(\delta_{max}\Delta\boldsymbol{X}^T(k)\boldsymbol{R}\Delta\boldsymbol{X}(k) \end{aligned}$$

$$
\begin{aligned}
&- \sum_{i=-\delta_{max}}^{-1} \Delta \boldsymbol{X}^T(k+i)\boldsymbol{R}\Delta \boldsymbol{X}(k+i))\\
&\le \mathbb{E}(\delta_{max}\Delta \boldsymbol{X}^T(k)\boldsymbol{R}\Delta \boldsymbol{X}(k)\\
&- \sum_{i=-\beta_k}^{-1} \Delta \boldsymbol{X}^T(k+i)\boldsymbol{R}\Delta \boldsymbol{X}(k+i))\\
&\le \mathbb{E}(\delta_{max}(\boldsymbol{X}(k+1)-\boldsymbol{X}(k))^T\boldsymbol{R}(\boldsymbol{X}(k+1)-\boldsymbol{X}(k))\\
&-(\boldsymbol{X}(k)-\boldsymbol{X}(k-\beta_k))^T\boldsymbol{R}(\boldsymbol{X}(k)-\boldsymbol{X}(k-\beta_k))).
\end{aligned} \tag{31}
$$

Using (23) in (31), eqn. (32), shown at the bottom of the next page, is obtained. Again,

$$
\begin{aligned}
&\mathbb{E}(\boldsymbol{Y}^T(k)\boldsymbol{Y}(k) - \gamma^2(\boldsymbol{W}^T(k)\boldsymbol{W}(k)) = \mathbb{E}[\boldsymbol{\eta}^T(K)]\\
&\times \begin{bmatrix} (\boldsymbol{I}_N\otimes\boldsymbol{C})^T(\boldsymbol{I}_N\otimes\boldsymbol{C}) & \boldsymbol{0} & \boldsymbol{0}\\ * & \boldsymbol{0} & \boldsymbol{0}\\ * & * & -\gamma^2\boldsymbol{I}_N \end{bmatrix}\mathbb{E}[\boldsymbol{\eta}(K)].
\end{aligned} \tag{33}
$$

By adding (29), (30), upper bound of $\mathbb{E}(V_3(k))$ (32) and (33) and for any non-zero $\mathbb{E}(\boldsymbol{\eta}(k))$, (27) will be satisfied when following holds:

$$
\begin{bmatrix} \boldsymbol{\pi}_{11} & \boldsymbol{\pi}_{12} & \boldsymbol{\pi}_{13}\\ * & \boldsymbol{\pi}_{22} & \boldsymbol{\pi}_{23}\\ * & * & \boldsymbol{\pi}_{33} \end{bmatrix} < \boldsymbol{0}, \tag{34}
$$

where, $\boldsymbol{\pi}_{11} = (\bar{\boldsymbol{A}}_d^T\boldsymbol{P}\bar{\boldsymbol{A}}_d - \boldsymbol{P} + \boldsymbol{Q} + \delta_{max}(\bar{\boldsymbol{A}}_d^T\boldsymbol{R}\bar{\boldsymbol{A}}_d - \bar{\boldsymbol{A}}_d^T\boldsymbol{R} - \boldsymbol{R}\boldsymbol{A}_d + \boldsymbol{R}) - \boldsymbol{R} + (\boldsymbol{I}_N\otimes\boldsymbol{C})^T(\boldsymbol{I}_N\otimes\boldsymbol{C})), \boldsymbol{\pi}_{12} = \bar{\boldsymbol{A}}_d^T\boldsymbol{P}(\tilde{\boldsymbol{L}}r\otimes\boldsymbol{B}_d\boldsymbol{K}) + \delta_{max}(\bar{\boldsymbol{A}}_d^T\boldsymbol{R}(\tilde{\boldsymbol{L}}r\otimes\boldsymbol{B}_d\boldsymbol{K}) - \boldsymbol{R}(\tilde{\boldsymbol{L}}r\otimes\boldsymbol{B}_d\boldsymbol{K})) + \boldsymbol{R}, \boldsymbol{\pi}_{13} = (\bar{\boldsymbol{A}}_d^T\boldsymbol{P}(\boldsymbol{I}_N\otimes\boldsymbol{B}_d) + \delta_{max}(\bar{\boldsymbol{A}}_d^T\boldsymbol{R}(\boldsymbol{I}_N\otimes\boldsymbol{B}_d) - \boldsymbol{R}(\boldsymbol{I}_N\otimes\boldsymbol{B}_d))), \boldsymbol{\pi}_{22} = (\tilde{\boldsymbol{L}}r\otimes\boldsymbol{B}_d\boldsymbol{K})^T\boldsymbol{P}(\tilde{\boldsymbol{L}}r\otimes\boldsymbol{B}_d\boldsymbol{K}) - \boldsymbol{Q} + \delta_{max}((\tilde{\boldsymbol{L}}r\otimes\boldsymbol{B}_d\boldsymbol{K})^T\boldsymbol{R}(\tilde{\boldsymbol{L}}r\otimes\boldsymbol{B}_d\boldsymbol{K})) - \boldsymbol{R}, \boldsymbol{\pi}_{23} = (\tilde{\boldsymbol{L}}r\otimes\boldsymbol{B}_d\boldsymbol{K})^T\boldsymbol{P}(\boldsymbol{I}_N\otimes\boldsymbol{B}_d) + \delta_{max}((\tilde{\boldsymbol{L}}r\otimes\boldsymbol{B}_d\boldsymbol{K})^T\boldsymbol{R}(\boldsymbol{I}_N\otimes\boldsymbol{B}_d)), \boldsymbol{\pi}_{33} = (\boldsymbol{I}_N\otimes\boldsymbol{B}_d)^T\boldsymbol{P}(\boldsymbol{I}_N\otimes\boldsymbol{B}_d) + \delta_{max}(\boldsymbol{I}_N\otimes\boldsymbol{B}_d)^T\boldsymbol{R}(\boldsymbol{I}_N\otimes\boldsymbol{B}_d) - \gamma^2\otimes\boldsymbol{I}_N$.

Using matrix factorisation, (34) can be re-written as (35), shown at the bottom of the next page and taking Schur complement [55] of (35) yields (36), shown at the bottom of the next page. Now, multiplying by $diag\{\boldsymbol{P}^{-1}, \boldsymbol{P}^{-1}, \boldsymbol{I}_N, \boldsymbol{I}_{3N}, \boldsymbol{I}_{3N}, \boldsymbol{I}_N\}$ in both sides of (36) and defining $\bar{\boldsymbol{P}} = \boldsymbol{P}^{-1} = \boldsymbol{I}_N\otimes\boldsymbol{P}_0{}^{-1}$, $\bar{\boldsymbol{R}} = \boldsymbol{R}^{-1} = \boldsymbol{I}_N\otimes\boldsymbol{R}_0{}^{-1}$, $\boldsymbol{P}^{-1}\boldsymbol{Q}\boldsymbol{P}^{-1} = \boldsymbol{\Xi}$, $\boldsymbol{P}^{-1}\boldsymbol{R}\boldsymbol{P}^{-1} = \boldsymbol{\Theta}$ and $\boldsymbol{K} = \boldsymbol{Z}\boldsymbol{P}_0$ yields (14).$\square$

C. Proof of Theorem 2

In LMI (14), the submatrices $\{\bar{\boldsymbol{P}}, \bar{\boldsymbol{Q}}, \bar{\boldsymbol{R}}, \boldsymbol{\Xi}, \boldsymbol{\Theta}, \boldsymbol{I}_N\otimes\boldsymbol{A}_d, \boldsymbol{I}_N\otimes\boldsymbol{B}_d, \boldsymbol{I}_N\otimes\boldsymbol{C}, \gamma^2\boldsymbol{I}_N\}$ are block diagonal matrices and $\tilde{\boldsymbol{L}}$ is symmetric matrix. Thus, an orthogonal matrix $\boldsymbol{\Psi}\in\mathbb{R}^{N\times N}$ will satisfy $\boldsymbol{\Psi}^T = \boldsymbol{\Psi}^{-1}$ such that there exist $\boldsymbol{\Psi}^{-1}\tilde{\boldsymbol{L}}\boldsymbol{\Psi} = \boldsymbol{D}$, where, $\boldsymbol{D}$ represents the diagonal and real matrix, i.e., $\boldsymbol{D} = diag\{\lambda_1,\lambda_2,\ldots,\lambda_N\}$ with $\lambda_i = \lambda_i(\mathcal{L}+\mathcal{P})$, $i = 1, 2, \ldots, N$, λ_i is the i^{th} real eigenvalue of $\tilde{\boldsymbol{L}} = (\mathcal{L}+\mathcal{P})$.

Now, define $\bar{\boldsymbol{\Psi}} = diag\{\bar{\boldsymbol{\Psi}}_0,\bar{\boldsymbol{\Psi}}_0,\bar{\boldsymbol{\Psi}}_0,\bar{\boldsymbol{\Psi}}_0,\bar{\boldsymbol{\Psi}}_0,\bar{\boldsymbol{\Psi}}_0\}$ and $\bar{\boldsymbol{\Psi}}^{-1} = diag\{\bar{\boldsymbol{\Psi}}_0^{-1},\bar{\boldsymbol{\Psi}}_0^{-1},\bar{\boldsymbol{\Psi}}_0^{-1},\bar{\boldsymbol{\Psi}}_0^{-1},\bar{\boldsymbol{\Psi}}_0^{-1},\bar{\boldsymbol{\Psi}}_0^{-1}\}$ with $\bar{\boldsymbol{\Psi}}_0 = \boldsymbol{\Psi}\otimes\boldsymbol{I}_3$ where n represents the order of the system (5), i.e., $n = 3$. Then the matrix $\tilde{\boldsymbol{\Pi}}$ can be defined as (37), shown at the bottom of the next page, where, $\tilde{\boldsymbol{A}_d} = ((\boldsymbol{I}_N\otimes\boldsymbol{A}_d)\bar{\boldsymbol{P}} + \tilde{\boldsymbol{L}}(1-r)\otimes\boldsymbol{B}_d\boldsymbol{Z})$. Now, using the properties of Kronecker product [41] in (37) yields (38), shown at the bottom of the next page.

Since $\boldsymbol{\Psi}$ is an orthogonal matrix satisfying satisfying $\boldsymbol{\Psi}^T = \boldsymbol{\Psi}^{-1}$ such that $\boldsymbol{\Psi}^{-1}\tilde{\boldsymbol{L}}\boldsymbol{\Psi} = \boldsymbol{D}$, therefore the following holds:

$$
\boldsymbol{\Pi} \Leftrightarrow \tilde{\boldsymbol{\Pi}} < \boldsymbol{0}. \tag{39}
$$

Moreover, it is observed that all the submatrices in LMI (38) are block diagonal. Therefore, (38) can be re-written with decomposed form for all $\lambda_i = \lambda_i(\mathcal{L}+\mathcal{P})$, $i = 1, 2, \ldots, N$, such that $\tilde{\boldsymbol{\Pi}} < \boldsymbol{0}$ iff (15) holds i.e. $\tilde{\boldsymbol{\Pi}}_i < \boldsymbol{0}$ where, λ_i represents the eigenvalues of $(\mathcal{L}+\mathcal{P})$. $\square$

$$
\begin{aligned}
&\mathbb{E}(\tilde{\boldsymbol{X}}(k+1))\\
&= \begin{bmatrix}
\boldsymbol{I}_N\otimes\boldsymbol{A}_d + (\mathcal{L}+\mathcal{P})(1-r)\otimes\boldsymbol{B}_d\boldsymbol{K} & \boldsymbol{0}_{3N\times3N} & \ldots & \boldsymbol{0}_{3N\times3N} & (\mathcal{L}+\mathcal{P})r\otimes\boldsymbol{B}_d\boldsymbol{K}\\
\boldsymbol{I}_{3N\times3N} & \boldsymbol{0}_{3N\times3N} & \ldots & \boldsymbol{0}_{3N\times3N} & \boldsymbol{0}_{3N\times3N}\\
\boldsymbol{0}_{3N\times3N} & \boldsymbol{I}_{3N\times3N} & \ldots & \boldsymbol{0}_{3N\times3N} & \boldsymbol{0}_{3N\times3N}\\
\vdots & \vdots & \ddots & \ddots & \vdots\\
\boldsymbol{0}_{3N\times3N} & \boldsymbol{0}_{3N\times3N} & \ldots & \boldsymbol{I}_{3N\times3N} & \boldsymbol{0}_{3N\times3N}
\end{bmatrix}\mathbb{E}(\tilde{\boldsymbol{X}}(k)) + \begin{bmatrix}\boldsymbol{I}_N\otimes\boldsymbol{B}_d\\ \boldsymbol{0}_{3N\times N}\\ \boldsymbol{0}_{3N\times N}\\ \vdots\\ \boldsymbol{0}_{3N\times N}\end{bmatrix}\mathbb{E}(\boldsymbol{W}(k)).
\end{aligned} \tag{24}
$$

$$
\begin{aligned}
G(z) = {}& T_s{}^3 z^{\delta}[\boldsymbol{I}_n\cdot(\tau z^{\delta+3} + (T_s-3\tau)z^{\delta+2} + (3\tau-2T_s)z^{\delta+1} + (T_s-\tau)z^{\delta}) + (\mathcal{L}+\mathcal{P})((K_a - K_v T_s + K_s T_s{}^2)T_s r - (2K_a\\
&-K_v T_s)T_s r z + K_a T_s r z^2 + (K_a - K_v T_s + K_s T_s{}^2)T_s(1-r)z^{\delta} + (K_v T_s - 2K_a)T_s(1-r)z^{\delta+1} + K_a T_s(1-r)z^{\delta+2})]^{-1}.
\end{aligned} \tag{25}
$$

$$
\mathbb{E}\{\Delta V_1(k)\} = \mathbb{E}[\boldsymbol{\eta}^T(K)]\begin{bmatrix}
\bar{\boldsymbol{A}}_d^T\boldsymbol{P}\bar{\boldsymbol{A}}_d - \boldsymbol{P} & \bar{\boldsymbol{A}}_d^T\boldsymbol{P}(\tilde{\boldsymbol{L}}r\otimes\boldsymbol{B}_d\boldsymbol{K}) & \bar{\boldsymbol{A}}_d^T\boldsymbol{P}(\boldsymbol{I}_N\otimes\boldsymbol{B}_d)\\
* & (\tilde{\boldsymbol{L}}r\otimes\boldsymbol{B}_d\boldsymbol{K})^T\boldsymbol{P}(\tilde{\boldsymbol{L}}r\otimes\boldsymbol{B}_d\boldsymbol{K}) & (\tilde{\boldsymbol{L}}r\otimes\boldsymbol{B}_d\boldsymbol{K})^T\boldsymbol{P}(\boldsymbol{I}_N\otimes\boldsymbol{B}_d)\\
* & * & (\boldsymbol{I}_N\otimes\boldsymbol{B}_d)^T\boldsymbol{P}(\boldsymbol{I}_N\otimes\boldsymbol{B}_d)
\end{bmatrix}\mathbb{E}[\boldsymbol{\eta}(K)]. \tag{29}
$$

D. Proof of Theorem 3

As shown in Theorem 2, the matrix $\tilde{\boldsymbol{L}} = (\mathcal{L} + \mathcal{P})$ is symmetric, thus there also exist an orthogonal matrix $\boldsymbol{\Psi} \in \mathbb{R}^{N\times N}$ with the satisfaction of $\boldsymbol{\Psi}^T = \boldsymbol{\Psi}^{-1}$ such that $\boldsymbol{\Psi}^{-1}\tilde{\boldsymbol{L}}\boldsymbol{\Psi} = \boldsymbol{D}$. Using this matrix property, the discrete time closed-loop transfer function (25) under random consecutive packet drop for the vehicle platoon system with undirected topology can be written as (40), shown at the top of the next page [9]. Eqn. (40) implies,

$$G(z) = \boldsymbol{\Psi}[diag\{G_1(z), G_2(z), \ldots, G_N(z)\}]\boldsymbol{\Psi}^{-1}, \quad (41)$$

with $G_i(z), i = 1, 2, \ldots, N$ as given in (16) where, $G_i(z)$ represents the closed-loop transfer function of i^{th} vehicle in a platoon and $\lambda_i = \lambda_i(\mathcal{L} + \mathcal{P})$, $i = 1, 2, \ldots, N$.

E. Proof of Statement 3.1 of Theorem 3

Using property of orthogonal matrix $\boldsymbol{\Psi}$ as detailed above, (41) can be represented as a block diagonal matrix. Therefore, it can be inferred that $G_i(z)$ will be asymptotically stable if and only if closed-loop poles of $G_i(z), i = 1, 2, \ldots, N$ are within a unit circle, i.e., $|z| < 1$.

$$\begin{aligned}
&\mathbb{E}\{\Delta V_3(k)\} \\
&= \mathbb{E}[\boldsymbol{\eta}^T(K)]\delta_{max}\begin{bmatrix} \bar{\boldsymbol{A}}_d^T\boldsymbol{R}\bar{\boldsymbol{A}}_d - \bar{\boldsymbol{A}}_d^T\boldsymbol{R} - \boldsymbol{R}\boldsymbol{A}_d + \boldsymbol{R} & \bar{\boldsymbol{A}}_d^T\boldsymbol{R}(\tilde{\boldsymbol{L}}r\otimes\boldsymbol{B}_d\boldsymbol{K}) - \boldsymbol{R}(\tilde{\boldsymbol{L}}r\otimes\boldsymbol{B}_d\boldsymbol{K}) & \bar{\boldsymbol{A}}_d^T\boldsymbol{R}(\boldsymbol{I}_N\otimes\boldsymbol{B}_d) - \boldsymbol{R}(\boldsymbol{I}_N\otimes\boldsymbol{B}_d) \\ * & (\tilde{\boldsymbol{L}}r\otimes\boldsymbol{B}_d\boldsymbol{K})^T\boldsymbol{R}(\tilde{\boldsymbol{L}}r\otimes\boldsymbol{B}_d\boldsymbol{K}) & (\tilde{\boldsymbol{L}}r\otimes\boldsymbol{B}_d\boldsymbol{K})^T\boldsymbol{R}(\boldsymbol{I}_N\otimes\boldsymbol{B}_d) \\ * & * & (\boldsymbol{I}_N\otimes\boldsymbol{B}_d)^T\boldsymbol{R}(\boldsymbol{I}_N\otimes\boldsymbol{B}_d) \end{bmatrix} \\
&\quad \times\mathbb{E}[\boldsymbol{\eta}(K)] + \mathbb{E}[\boldsymbol{\eta}^T(K)]\begin{bmatrix} -\boldsymbol{R} & \boldsymbol{R} & \boldsymbol{0} \\ * & -\boldsymbol{R} & \boldsymbol{0} \\ * & * & \boldsymbol{0}\end{bmatrix}\mathbb{E}[\boldsymbol{\eta}(K)]. \qquad (32)
\end{aligned}$$

$$\begin{aligned}
&\begin{bmatrix} \boldsymbol{Q} - \boldsymbol{P} - \boldsymbol{R} & \boldsymbol{R} & \boldsymbol{0} \\ * & -\boldsymbol{Q} - \boldsymbol{R} & \boldsymbol{0} \\ * & * & -\gamma^2\boldsymbol{I}_N \end{bmatrix} + \begin{bmatrix} (\boldsymbol{I}_N\otimes\boldsymbol{C})^T \\ \boldsymbol{0} \\ \boldsymbol{0}\end{bmatrix}\begin{bmatrix}(\boldsymbol{I}_N\otimes\boldsymbol{C}) & \boldsymbol{0} & \boldsymbol{0}\end{bmatrix} + \begin{bmatrix} \bar{\boldsymbol{A}}_d^T \\ (\tilde{\boldsymbol{L}}r\otimes\boldsymbol{B}_d\boldsymbol{K})^T \\ (\boldsymbol{I}_N\otimes\boldsymbol{B}_d)^T \end{bmatrix}\boldsymbol{P} \\
&\quad\times\begin{bmatrix}\bar{\boldsymbol{A}}_d & (\tilde{\boldsymbol{L}}r\otimes\boldsymbol{B}_d\boldsymbol{K}) & (\boldsymbol{I}_N\otimes\boldsymbol{B}_d)\end{bmatrix} + \delta_{max}\begin{bmatrix} (\bar{\boldsymbol{A}}_d - \boldsymbol{I}_{3N})^T \\ (\tilde{\boldsymbol{L}}r\otimes\boldsymbol{B}_d\boldsymbol{K})^T \\ (\boldsymbol{I}_N\otimes\boldsymbol{B}_d)^T\end{bmatrix}\boldsymbol{R}\begin{bmatrix}(\bar{\boldsymbol{A}}_d - \boldsymbol{I}_{3N}) & (\tilde{\boldsymbol{L}}r\otimes\boldsymbol{B}_d\boldsymbol{K}) & (\boldsymbol{I}_N\otimes\boldsymbol{B}_d)\end{bmatrix} < \boldsymbol{0}. \qquad (35)
\end{aligned}$$

$$\begin{bmatrix} \boldsymbol{Q} - \boldsymbol{P} - \boldsymbol{R} & * & * & * & * & * \\ \boldsymbol{R} & -\boldsymbol{Q} - \boldsymbol{R} & * & * & * & * \\ \boldsymbol{0} & \boldsymbol{0} & -\gamma^2\boldsymbol{I}_N & * & * & * \\ \bar{\boldsymbol{A}}_d & \tilde{\boldsymbol{L}}r\otimes\boldsymbol{B}_d\boldsymbol{K} & \boldsymbol{I}_N\otimes\boldsymbol{B}_d & -\boldsymbol{P}^{-1} & * & * \\ \delta_{max}(\bar{\boldsymbol{A}}_d - \boldsymbol{I}_{3N}) & \delta_{max}(\tilde{\boldsymbol{L}}r\otimes\boldsymbol{B}_d\boldsymbol{K}) & \delta_{max}(\boldsymbol{I}_N\otimes\boldsymbol{B}_d) & \boldsymbol{0} & -\delta_{max}\boldsymbol{R}^{-1} & * \\ (\boldsymbol{I}_N\otimes\boldsymbol{C}) & \boldsymbol{0} & \boldsymbol{0} & \boldsymbol{0} & \boldsymbol{0} & -\boldsymbol{I}_N \end{bmatrix} < \boldsymbol{0}. \qquad (36)$$

$$\begin{aligned}
\tilde{\boldsymbol{\Pi}} &= \bar{\boldsymbol{\Psi}}^{-1}\boldsymbol{\Pi}\bar{\boldsymbol{\Psi}} \\
&= \begin{bmatrix} \bar{\boldsymbol{\Psi}}_0^{-1}(\boldsymbol{\Xi} - \bar{\boldsymbol{P}} - \boldsymbol{\Theta})\bar{\boldsymbol{\Psi}}_0 & * & * & * & * & * \\ \bar{\boldsymbol{\Psi}}_0^{-1}\boldsymbol{\Theta}\bar{\boldsymbol{\Psi}}_0 & \bar{\boldsymbol{\Psi}}_0^{-1}(-\boldsymbol{\Xi} - \boldsymbol{\Theta})\bar{\boldsymbol{\Psi}}_0 & * & * & * & * \\ \boldsymbol{0} & \boldsymbol{0} & -\bar{\boldsymbol{\Psi}}_0^{-1}(\gamma^2\boldsymbol{I}_N)\bar{\boldsymbol{\Psi}}_0 & * & * & * \\ \bar{\boldsymbol{\Psi}}_0^{-1}\tilde{\boldsymbol{A}}_d\bar{\boldsymbol{\Psi}}_0 & \bar{\boldsymbol{\Psi}}_0^{-1}(\tilde{\boldsymbol{L}}r\otimes\boldsymbol{B}_d\boldsymbol{Z})\bar{\boldsymbol{\Psi}}_0 & \bar{\boldsymbol{\Psi}}_0^{-1}(\boldsymbol{I}_N\otimes\boldsymbol{B}_d)\bar{\boldsymbol{\Psi}}_0 & -\bar{\boldsymbol{\Psi}}_0^{-1}\bar{\boldsymbol{P}}\bar{\boldsymbol{\Psi}}_0 & * & * \\ \bar{\boldsymbol{\Psi}}_0^{-1}(\delta_{max}(\tilde{\boldsymbol{A}}_d - \bar{\boldsymbol{P}}))\bar{\boldsymbol{\Psi}}_0 & \bar{\boldsymbol{\Psi}}_0^{-1}\delta_{max}(\tilde{\boldsymbol{L}}r\otimes\boldsymbol{B}_d\boldsymbol{Z})\bar{\boldsymbol{\Psi}}_0 & \bar{\boldsymbol{\Psi}}_0^{-1}\delta_{max}(\boldsymbol{I}_N\otimes\boldsymbol{B}_d)\bar{\boldsymbol{\Psi}}_0 & \boldsymbol{0} & -\bar{\boldsymbol{\Psi}}_0^{-1}\delta_{max}\bar{\boldsymbol{R}}\bar{\boldsymbol{\Psi}}_0 & * \\ \bar{\boldsymbol{\Psi}}_0^{-1}((\boldsymbol{I}_N\otimes\boldsymbol{C})\bar{\boldsymbol{P}})\bar{\boldsymbol{\Psi}}_0 & \boldsymbol{0} & \boldsymbol{0} & \boldsymbol{0} & \boldsymbol{0} & -\bar{\boldsymbol{\Psi}}_0^{-1}\boldsymbol{I}_N\bar{\boldsymbol{\Psi}}_0 \end{bmatrix} \\
&< \boldsymbol{0}. \qquad (37)
\end{aligned}$$

$$\tilde{\boldsymbol{\Pi}} = \begin{bmatrix} \boldsymbol{I}_N\otimes\boldsymbol{\Xi}_0 - \boldsymbol{I}_N\otimes\bar{\boldsymbol{P}}_0 - \boldsymbol{I}_N\otimes\boldsymbol{\Theta}_0 & * & * & * & * & * \\ \boldsymbol{I}_N\otimes\boldsymbol{\Theta}_0 & -\boldsymbol{I}_N\otimes\boldsymbol{\Xi}_0 - \boldsymbol{I}_N\otimes\boldsymbol{\Theta}_0 & * & * & * & * \\ \boldsymbol{0} & \boldsymbol{0} & -\gamma^2\boldsymbol{I}_N & * & * & * \\ ((\boldsymbol{I}_N\otimes\boldsymbol{A}_d)(\boldsymbol{I}_N\otimes\bar{\boldsymbol{P}}_0) + \boldsymbol{D}(1-r)\otimes\boldsymbol{B}_d\boldsymbol{Z}) & \boldsymbol{D}r\otimes\boldsymbol{B}_d\boldsymbol{Z} & \boldsymbol{I}_N\otimes\boldsymbol{B}_d & -\boldsymbol{I}_N\otimes\bar{\boldsymbol{P}}_0 & * & * \\ \delta_{max}((\boldsymbol{I}_N\otimes\boldsymbol{A}_d)(\boldsymbol{I}_N\otimes\bar{\boldsymbol{P}}_0) + \boldsymbol{D}(1-r)\otimes\boldsymbol{B}_d\boldsymbol{Z} - \boldsymbol{I}_N\otimes\bar{\boldsymbol{P}}_0) & \delta_{max}\boldsymbol{D}r\otimes\boldsymbol{B}_d\boldsymbol{Z} & \boldsymbol{I}_N\otimes\boldsymbol{B}_d\delta_{max} & \boldsymbol{0} & -\delta_{max}(\boldsymbol{I}_N\otimes\bar{\boldsymbol{R}}_0) & * \\ (\boldsymbol{I}_N\otimes\boldsymbol{C})(\boldsymbol{I}_N\otimes\bar{\boldsymbol{P}}_0) & \boldsymbol{0} & \boldsymbol{0} & \boldsymbol{0} & \boldsymbol{0} & -\boldsymbol{I}_N \end{bmatrix} < \boldsymbol{0}. \qquad (38)$$

$$G(z) = \boldsymbol{\Psi}(T_s{}^3 z^{\delta}[\boldsymbol{I}_n \cdot (\tau z^{\delta+3} + (T_s - 3\tau)z^{\delta+2} + (3\tau - 2T_s)z^{\delta+1} + (T_s - \tau)z^{\delta}) + \boldsymbol{D}((K_a - K_v T_s + K_s T_s{}^2)T_s r \\ -(2K_a - K_v T_s)T_s r z + K_a T_s r z^2 + (K_a - K_v T_s + K_s T_s{}^2)T_s(1-r)z^{\delta} \\ +(K_v T_s - 2K_a)T_s(1-r)z^{\delta+1} + K_a T_s(1-r)z^{\delta+2})]^{-1})\boldsymbol{\Psi}^{-1}. \quad (40)$$

F. Proof of Statement 3.2 and 3.3 of Theorem 3

The characteristic polynomial (17) can be written with $\delta_{max} = \delta$ as:

$$\nabla(z) = b_0 z^{\delta+3} + b_1 z^{\delta+2} + b_2 z^{\delta+1} + \ldots + b_{n-2}z^2 \\ + b_{n-1}z + b_n, \quad (42)$$

where, $b_0 = 1$, $b_1 = \frac{(T_s - 3\tau) + \lambda_i(K_a T_s(1-r))}{\tau}$, $b_2 = \frac{(3\tau - 2T_s) + \lambda_i(K_v T_s - 2K_a)(1-r)T_s}{\tau}$, $b_3 = \frac{(T_s - \tau) + \lambda_i(K_a - K_v T_s + K_s T_s^2)(1-r)T_s}{\tau}$, $b_{n-2} = \frac{\lambda_i K_a T_s r}{\tau}$, $b_{n-1} = \frac{\lambda_i(K_v T_s - 2K_a)T_s r}{\tau}$, $b_n = \frac{\lambda_i(K_a - K_v T_s + K_s T_s^2)r T_s}{\tau}$ and $b_4 = b_5 = \ldots = b_{n-3} = 0$.

The eqn. (42) is a Schur polynomial if $b_0 > b_n$ [56]. It is seen from (42) that if λ_i goes to zero then three roots are moving towards zero as $\mathcal{O}(\lambda_i)$ and rest of the roots are with certain value, depending on the parameters $\{T_s, \tau\}$.

G. Proof of Theorem 4 and 5

It can be observed from Theorem 3 and (17) that closed-loop system is internally stable if all the characteristic roots of (18),(19) and (20), (21) satisfy $|z| < 1$ for both minimum and maximum eigenvalue, i.e. λ_{min} and of λ_{max} when homogeneous platoon is with BPF and BPLF topologies, respectively. It was proven in Theorem 2 for homogeneous platoon system with BPF and BPLF topologies in [6] that if $i \ll N$ and if $i = N$ then following holds:

$$\frac{1}{N^2} \leq \lambda_i(\mathcal{L}_{BPF} + \mathcal{P}_{BPF}) \leq 4, \quad (43a)$$

$$1 \leq \lambda_i(\mathcal{L}_{BPLF} + \mathcal{P}_{BPLF}) \leq 1 + 4 = 5, \quad (43b)$$

respectively. Using boundary values of $\lambda_i(\mathcal{L}_{BPF} + \mathcal{P}_{BPF})$ and $\lambda_i(\mathcal{L}_{BPLF} + \mathcal{P}_{BPLF})$ from (43), i.e., lower and upper bound $\lambda_{min}(\mathcal{L}_{BPF} + \mathcal{P}_{BPF})$, $\lambda_{max}(\mathcal{L}_{BPF} + \mathcal{P}_{BPF})$ and $\lambda_{min}(\mathcal{L}_{BPLF} + \mathcal{P}_{BPLF})$, $\lambda_{max}(\mathcal{L}_{BPLF} + \mathcal{P}_{BPLF})$ in (17) yields (18),(19) and (20), (21), respectively.□

REFERENCES

[1] D. Jia and D. Ngoduy, "Enhanced cooperative car-following traffic model with the combination of V2V and V2I communication," *Transp. Res. B, Methodol.*, vol. 90, pp. 172–191, Aug. 2016.

[2] S. Li *et al.*, "Distributed platoon control under topologies with complex eigenvalues: Stability analysis and controller synthesis," *IEEE Trans. Control Syst. Technol.*, vol. 27, no. 1, pp. 206–220, Jan. 2019.

[3] J. K. Hedrick, M. Tomizuka, and P. Varaiya, "Control issues in automated highway systems," *IEEE Control Syst.*, vol. 14, no. 6, pp. 21–32, Dec. 1994.

[4] U. Montanaro *et al.*, "Towards connected autonomous driving: Review of use-cases," *Vehicle Syst. Dyn.*, vol. 57, no. 6, pp. 779–814, 2019.

[5] G. J. L. Naus, R. P. A. Vugts, J. Ploeg, M. J. G. van de Molengraft, and M. Steinbuch, "String-stable CACC design and experimental validation: A frequency-domain approach," *IEEE Trans. Veh. Technol.*, vol. 59, no. 9, pp. 4268–4279, Nov. 2010.

[6] Y. Zheng, S. Li, J. Wang, D. Cao, and K. Li, "Stability and scalability of homogeneous vehicular platoon: Study on the influence of information flow topologies," *IEEE Trans. Intell. Transp. Syst.*, vol. 17, no. 1, pp. 14–26, Jan. 2015.

[7] Y. Zheng, S. E. Li, K. Li, and W. Ren, "Platooning of connected vehicles with undirected topologies: Robustness analysis and distributed H-infinity controller synthesis," *IEEE Trans. Intell. Transp. Syst.*, vol. 19, no. 5, pp. 1353–1364, May 2018.

[8] S. E. Li *et al.*, "Dynamical modeling and distributed control of connected and automated vehicles: Challenges and opportunities," *IEEE Intell. Transp. Syst. Mag.*, vol. 9, no. 3, pp. 46–58, Jul. 2017.

[9] K. Halder, U. Montanaro, S. Dixit, M. Dianati, A. Mouzakitis, and S. Fallah, "Distributed H_∞ controller design and robustness analysis for vehicle platooning under random packet drop," *IEEE Trans. Intell. Transp. Syst.*, vol. 23, no. 5, pp. 4373–4386, May 2022.

[10] U. Montanaro, S. Fallah, M. Dianati, D. Oxtoby, T. Mizutani, and A. Mouzakitis, "On a fully self-organizing vehicle platooning supported by cloud computing," in *Proc. 5th Int. Conf. Internet Things, Syst., Manage. Secur.*, Oct. 2018, pp. 295–302.

[11] Y. Zheng, S. Li, K. Li, and L.-Y. Wang, "Stability margin improvement of vehicular platoon considering undirected topology and asymmetric control," *IEEE Trans. Control Syst. Technol.*, vol. 24, no. 4, pp. 1253–1265, Jul. 2016.

[12] F. Gao, F. Lin, and B. Liiu, "Distributed H_∞ control of platoon interacted by switching and undirected topology," *Int. J. Automot. Technol.*, vol. 21, pp. 259–268, Feb. 2020.

[13] J.-W. Kwon and D. Chwa, "Adaptive bidirectional platoon control using a coupled sliding mode control method," *IEEE Trans. Intell. Transp. Syst.*, vol. 15, no. 5, pp. 2040–2048, Oct. 2014.

[14] K. Halder *et al.*, "Distributed controller design for vehicle platooning under packet drop scenario," in *Proc. IEEE 23rd Int. Conf. Intell. Transp. Syst. (ITSC)*, Sep. 2020, pp. 1–8.

[15] C. Lei, E. M. van Eenennaam, W. K. Wolterink, G. Karagiannis, G. Heijenk, and J. Ploeg, "Impact of packet loss on CACC string stability performance," in *Proc. 11th Int. Conf. ITS Telecommun.*, Aug. 2011, pp. 381–386.

[16] S. E. Li, Y. Zheng, K. Li, L.-Y. Wang, and H. Zhang, "Platoon control of connected vehicles from a networked control perspective: Literature review, component modeling, and controller synthesis," *IEEE Trans. Veh. Technol.*, early access, Jul. 6, 2018, doi: 10.1109/TVT.2017.2723881.

[17] R. Trestian, G.-M. Muntean, and O. Ormond, "Signal strength-based adaptive multimedia delivery mechanism," in *Proc. IEEE 34th Conf. Local Comput. Netw.*, Oct. 2009, pp. 297–300.

[18] C. Lei, E. M. van Eenennaam, W. Klein Wolterink, J. Ploeg, G. Karagiannis, and G. Heijenk, "Evaluation of CACC string stability using SUMO, simulink, and OMNeT++," *EURASIP J. Wireless Commun. Netw.*, vol. 2012, no. 1, p. 116, Dec. 2012.

[19] L. Xu, L. Y. Wang, G. Yin, and H. Zhang, "Impact of communication erasure channels on the safety of highway vehicle platoons," *IEEE Trans. Intell. Transp. Syst.*, vol. 16, no. 3, pp. 1456–1468, Jun. 2015.

[20] Y. Zheng, S. E. Li, K. Li, F. Borrelli, and J. K. Hedrick, "Distributed model predictive control for heterogeneous vehicle platoons under unidirectional topologies," *IEEE Trans. Control Syst. Technol.*, vol. 25, no. 3, pp. 899–910, May 2017.

[21] H. Zhou, R. Saigal, F. Dion, and L. Yang, "Vehicle platoon control in high-latency wireless communications environment: Model predictive control method," *Transp. Res. Rec., J. Transp. Res. Board*, vol. 2324, no. 1, pp. 81–90, 2012.

[22] B. Peng, D. Yu, H. Zhou, X. Xiao, and Y. Fang, "A platoon control strategy for autonomous vehicles based on sliding-mode control theory," *IEEE Access*, vol. 8, pp. 81776–81788, 2020.

[23] C. Zhao, L. Cai, and P. Cheng, "Stability analysis of vehicle platooning with limited communication range and random packet losses," *IEEE Internet Things J.*, vol. 8, no. 1, pp. 262–277, Jan. 2021.

[24] S. Wen and G. Guo, "Control of leader-following vehicle platoons with varied communication range," *IEEE Trans. Intell. Vehicles*, vol. 5, no. 2, pp. 240–250, Jun. 2020.

[25] A. Elahi, A. Alfi, and H. Modares, "H_∞ consensus of homogeneous vehicular platooning systems with packet dropout and communication delay," *IEEE Trans. Syst., Man, Cybern. Syst.*, vol. 52, no. 6, pp. 3680–3691, Jun. 2022.

[26] Y. Zheng, Y. Bian, S. Li, and S. E. Li, "Cooperative control of heterogeneous connected vehicles with directed acyclic interactions," *IEEE Intell. Transp. Syst. Mag.*, vol. 13, no. 2, pp. 127–141, Summer 2021.

[27] L. Xu, W. Zhuang, G. Yin, C. Bian, and H. Wu, "Modeling and robust control of heterogeneous vehicle platoons on curved roads subject to disturbances and delays," *IEEE Trans. Veh. Technol.*, vol. 68, no. 12, pp. 11551–11564, Sep. 2019.

[28] L. Xu, W. Zhuang, G. Yin, and C. Bian, "Stable longitudinal control of heterogeneous vehicular platoon with disturbances and information delays," *IEEE Access*, vol. 6, pp. 69794–69806, 2018.

[29] Y. Tang, M. Yan, P. Yang, and L. Zuo, "Consensus based control algorithm for vehicle platoon with packet losses," in *Proc. 37th Chin. Control Conf. (CCC)*, Jul. 2018, pp. 7684–7689.

[30] H. Guo, J. Liu, Q. Dai, H. Chen, Y. Wang, and W. Zhao, "A distributed adaptive triple-step nonlinear control for a connected automated vehicle platoon with dynamic uncertainty," *IEEE Internet Things J.*, vol. 7, no. 5, pp. 3861–3871, May 2020.

[31] P. Barooah, P. G. Mehta, and J. P. Hespanha, "Mistuning-based control design to improve closed-loop stability margin of vehicular platoons," *IEEE Trans. Autom. Control*, vol. 54, no. 9, pp. 2100–2113, Sep. 2009.

[32] H. Hao, P. Barooah, and P. G. Mehta, "Stability margin scaling laws for distributed formation control as a function of network structure," *IEEE Trans. Autom. Control*, vol. 56, no. 4, pp. 923–929, Apr. 2011.

[33] B. Caiazzo, D. G. Lui, A. Petrillo, and S. Santini, "Distributed double-layer control for coordination of multiplatoons approaching road restriction in the presence of IoV communication delays," *IEEE Internet Things J.*, vol. 9, no. 6, pp. 4090–4109, Mar. 2022.

[34] A. Ibrahim, D. Goswami, H. Li, I. M. Soroa, and T. Basten, "Multi-layer multi-rate model predictive control for vehicle platooning under IEEE 802.11 p," *Transp. Res. C, Emerg. Technol.*, vol. 124, Mar. 2021, Art. no. 102905.

[35] J. Wang, F. Ma, Y. Yang, J. Nie, B. Aksun-Guvenc, and L. Guvenc, "Adaptive event-triggered platoon control under unreliable communication links," *IEEE Trans. Intell. Transp. Syst.*, vol. 23, no. 3, pp. 1924–1935, Mar. 2022.

[36] C. Zhao, X. Duan, L. Cai, and P. Cheng, "Vehicle platooning with non-ideal communication networks," *IEEE Trans. Veh. Technol.*, vol. 70, no. 1, pp. 18–32, Jan. 2021.

[37] S. Wen and G. Guo, "Cooperative control and communication of connected vehicles considering packet dropping rate," *Int. J. Syst. Sci.*, vol. 49, no. 13, pp. 2808–2825, Oct. 2018.

[38] G. Guo and W. Yue, "Hierarchical platoon control with heterogeneous information feedback," *IET Control Theory Appl.*, vol. 5, no. 15, pp. 1766–1781, 2011.

[39] S. Öncü, J. Ploeg, N. van de Wouw, and H. Nijmeijer, "Cooperative adaptive cruise control: Network-aware analysis of string stability," *IEEE Trans. Intell. Transp. Syst.*, vol. 15, no. 4, pp. 1527–1537, Aug. 2014.

[40] M. R. Hidayatullah and J.-C. Juang, "Centralized and distributed control framework under homogeneous and heterogeneous platoon," *IEEE Access*, vol. 9, pp. 49629–49648, 2021.

[41] Y.-J. Pan, H. Werner, Z. Huang, and M. Bartels, "Distributed cooperative control of leader–follower multi-agent systems under packet dropouts for quadcopters," *Syst. Control Lett.*, vol. 106, pp. 47–57, Aug. 2017.

[42] K. Ogata *et al.*, *Discrete-Time Control Systems*, vol. 2. Englewood Cliffs, NJ, USA: Prentice-Hall, 1995.

[43] G. F. Franklin *et al.*, *Digital Control of Dynamic Systems*, vol. 3. Reading, MA, USA: Addison-Wesley, 1998.

[44] K. Halder, S. Das, and A. Gupta, "Transformation of LQR weights for discretization invariant performance of PI/PID dominant pole placement controllers," *Robotica*, vol. 38, no. 2, pp. 271–298, Feb. 2020.

[45] S. Darbha, K. R. Rajagopal, and V. Tyagi, "A review of mathematical models for the flow of traffic and some recent results," *Nonlinear Anal., Theory, Methods Appl.*, vol. 69, no. 3, pp. 950–970, Aug. 2008.

[46] H. Chehardoli and A. Ghasemi, "Adaptive centralized/decentralized control and identification of 1-D heterogeneous vehicular platoons based on constant time headway policy," *IEEE Trans. Intell. Transp. Syst.*, vol. 19, no. 10, pp. 3376–3386, Oct. 2018.

[47] J. Hu, P. Bhowmick, F. Arvin, A. Lanzon, and B. Lennox, "Cooperative control of heterogeneous connected vehicle platoons: An adaptive leader-following approach," *IEEE Robot. Autom. Lett.*, vol. 5, no. 2, pp. 977–984, Apr. 2020.

[48] Z. Wang, F. Yang, D. W. C. Ho, and X. Liu, "Robust H_∞ control for networked systems with random packet losses," *IEEE Trans. Syst., Man, Cybern. B, Cybern.*, vol. 37, no. 4, pp. 916–924, Aug. 2007.

[49] K. Halder, S. Das, S. Dasgupta, S. Banerjee, and A. Gupta, "Controller design for networked control systems-an approach based on L_2 induced norm," *Nonlinear Anal., Hybrid Syst.*, vol. 19, pp. 134–145, Feb. 2016.

[50] K. Halder, D. Bose, and A. Gupta, "Stability and performance analysis of networked control systems: A lifted sample-time approach with L_2 induced norm," *ISA Trans.*, vol. 86, pp. 62–72, Mar. 2019.

[51] J. Lofberg, "YALMIP: A toolbox for modeling and optimization in MATLAB," in *Proc. IEEE Int. Conf. Robot. Autom.*, Sep. 2004, pp. 284–289.

[52] J. F. Sturm, "Using SeDuMi 1.02, a MATLAB toolbox for optimization over symmetric cones," *Optim. Methods Softw.*, vol. 11, nos. 1–4, pp. 625–653, 1999.

[53] K. Halder, S. Das, and A. Gupta, "Time delay handling in dominant pole placement with PID controllers to obtain stability regions using random sampling," *Int. J. Control*, vol. 94, no. 12, pp. 3384–3405, Dec. 2021.

[54] P. Park, S. C. Ergen, C. Fischione, C. Lu, and K. H. Johansson, "Wireless network design for control systems: A survey," *IEEE Commun. Surveys Tuts.*, vol. 20, no. 2, pp. 978–1013, 2nd Quart., 2018.

[55] S. Boyd, L. El Ghaoui, E. Feron, and V. Balakrishnan, *Linear Matrix Inequalities in System and Control Theory*. Philadelphia, PA, USA: SIAM, 1994.

[56] S. P. Bhattacharyya, H. Chapellat, and L. H. Keel, *Robust Control: The Parametric Approach*. Upper Saddle River, NJ, USA: Prentice-Hall, 1995.

Kaushik Halder received the B.Tech. degree in electronics and instrumentation engineering from the Haldia Institute of Technology, Haldia, India, in 2008, and the M.E. degree in power engineering and the Ph.D. degree in engineering from Jadavpur University, Kolkata, India, in 2010 and 2018, respectively. He was an Assistant Professor in electronics and instrumentation engineering with the National Institute of Science and Technology, Brahmapur, India, from 2010 to 2013. He was a Post-Doctoral Researcher with the Department of Mechanical Engineering Sciences, University of Surrey, U.K., from 2019 to 2021. He is currently working as a Research Associate with The University of Edinburgh, U.K. He has authored or coauthored more than 25 research papers in refereed scientific journals and conferences. His research interests include control theory, networked control systems, and control of autonomous vehicles and intelligent systems.

Lee Gillam received the Ph.D. degree in artificial intelligence from the University of Surrey in 2004. He is currently a Reader with the Department of Computer Science, University of Surrey, a Chartered IT Professional Fellow of the British Computer Society (FBCS CITP), and a member of the EPSRC Peer Review College. He is the Founding Editor-in-Chief of *Journal of Cloud Computing Advances, Systems and Applications* (JoCCASA) (SpringerOpen), with its first articles in April 2012, and which followed on from co-editorship of the first Springer book on cloud computing in 2010. He has both led and contributed to government-funded research projects relating to cloud computing and started three companies that are variously exploiting, such research. He has been the coauthor of reports for EPSRC on cloud computing (research use cases, and costs), and has been teaching a bespoke module on cloud computing to master's students since 2010.

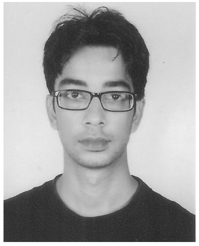

Shilp Dixit received the M.Sc. degree (Hons.) in automotive technology from The Eindhoven University of Technology, Eindhoven, The Netherlands, in 2015, and the Ph.D. degree in automotive engineering from the University of Surrey, U.K., in 2020. From 2010 to 2012, he worked in the field of technology consulting at Deloitte Consulting LLP, before making the switch to vehicle dynamics and control in 2012. Since he has also worked as a Researcher at Tata Motors Ltd., Flanders Make, and Arrival Ltd. He is currently working as a Senior Control Engineer at Vay Technology GmbH. His research interests are control of mechatronics systems, vehicle dynamics and control, trajectory planning and tracking for autonomous vehicles, and intelligent vehicles.

Alexandros Mouzakitis is currently the Head of the Electrical, Electronics and Software Engineering Research Department, Jaguar Land Rover. He has over 15 years of technological and managerial experience, especially in the area of automotive embedded systems. In his current role, he is responsible for leading a multidisciplinary research and technology department dedicated to deliver a portfolio of advanced research projects in the areas of human–machine interface, digital transformation, self-learning vehicle, smart/connected systems, and onboard/off board data platforms. In his previous position within JLR, he served as the Head of the Model-Based Product Engineering Department responsible for model-based development and automated testing standards and processes.

Saber Fallah is currently an Associate Professor with the University of Surrey. He is also the Director of the Connected and Autonomous Vehicles Laboratory (CAV-Laboratory), Department of Mechanical Engineering Sciences. Since joining the University of Surrey, he has been contributed to securing research funding from EPSRC, Innovate U.K., EU, KTP, and industry. His work has contributed to the state-of-the-art research in the areas of connected autonomous vehicles and advanced driver assistance systems. So far, his research has produced four patents and more than 40 peer reviewed publications in high-quality journals and well-known conferences. He is also the coauthor of a textbook titled *Electric and Hybrid Vehicles: Technologies, Modeling and Control: A Mechatronics Approach* (John Wiley, 2014). The book addresses the fundamentals of mechatronic design in hybrid and electric vehicles. Moreover, he is the co-editor of the book of conference proceedings resulted from the organization of the TAROS 2017 conference published by Springer in 2017.